LBL-18793
Preprint c.2

Lawrence Berkeley Laboratory

UNIVERSITY OF CALIFORNIA

RECEIVED
LAWRENCE
BERKELEY LABORATORY

FEB 11 1985

LIBRARY AND
DOCUMENTS SECTION

APPLIED SCIENCE DIVISION

Submitted to Chemical Engineering Communications

ZINC ELECTRODE CYCLE-LIFE PERFORMANCE IN ALKALINE ELECTROLYTES HAVING REDUCED ZINC SPECIES SOLUBILITY

J.T. Nichols, F.R. McLarnon, and E.J. Cairns

December 1984

TWO-WEEK LOAN COPY
This is a Library Circulating Copy
which may be borrowed for two weeks.

APPLIED SCIENCE
DIVISION

LBL-18793
c.2

Prepared for the U.S. Department of Energy under Contract DE-AC03-76SF00098

DISCLAIMER

This document was prepared as an account of work sponsored by the United States Government. While this document is believed to contain correct information, neither the United States Government nor any agency thereof, nor the Regents of the University of California, nor any of their employees, makes any warranty, express or implied, or assumes any legal responsibility for the accuracy, completeness, or usefulness of any information, apparatus, product, or process disclosed, or represents that its use would not infringe privately owned rights. Reference herein to any specific commercial product, process, or service by its trade name, trademark, manufacturer, or otherwise, does not necessarily constitute or imply its endorsement, recommendation, or favoring by the United States Government or any agency thereof, or the Regents of the University of California. The views and opinions of authors expressed herein do not necessarily state or reflect those of the United States Government or any agency thereof or the Regents of the University of California.

LBL-18793

ZINC ELECTRODE CYCLE-LIFE PERFORMANCE

IN

ALKALINE ELECTROLYTES HAVING REDUCED ZINC SPECIES SOLUBILITY

by

James T. Nichols,* Frank R. McLarnon and Elton J. Cairns

Applied Science Division
Lawrence Berkeley Laboratory

and

Department of Chemical Engineering
University of California
Berkeley, California 94720

Revised manuscript submitted to Chemical Engineering Communications

December 11, 1984

This work was supported by the Assistant Secretary for Conservation and Renewable Energy, Office of Energy Systems Research, Energy Storage Division of the U.S. Department of Energy under Contract No. DE-AC03-76SF00098.

---

* The Air Force Rocket Propulsion Laboratory, Edwards Air Force Base, California

ABSTRACT

Electrolytes having 3.5M hydroxide-ion concentration were tested in 1.35Ah Zn/NiOOH cells to evaluate their ability to reduce the extent of zinc species migration and slow the rate of cell capacity decline. Alkaline-fluoride and alkaline-borate electrolytes, in which ZnO solubility is approximately 25% of that in standard 7.4M KOH electrolyte, exhibited 0.09-0.14%/cycle zinc-electrode area loss, which may be compared to a value of 0.46%/cycle observed in standard electrolyte. In addition, no zinc penetration of the separator occurred in cells that employed alkaline-fluoride and alkaline-borate electrolytes, even when zinc-electrode overpotentials reached 290mV at the end of charge. Less than 2% of the zinc remaining after cycling was electrochemically inactive.

INTRODUCTION

Zinc is an attractive negative electrode material for use in secondary batteries with aqueous electrolytes because of its relative abundance, low equivalent weight, high coulombic efficiency, resistance to corrosion, and reversible electrochemical behavior. Pasted, polymer-bonded zinc electrodes have been employed in rechargeable Zn/NiOOH, Zn/AgO and Zn/air cells with 30-45 wt% KOH electrolyte. These cells offer very attractive values of specific energy (60-150 Wh/kg) and specific power (100-500 W/kg), and they are viable candidates for a number of applications where high performance is important. However, these cells display limited lifetimes, typically less than 400 deep-discharge cycles. These short lifetimes are usually the result of problems with the zinc electrode: active-material redistribution (shape change), densification and/or passivation can lead to a rapid decline in cell capacity; and dendritic zinc growth can lead to cell failure by shorting. Active-material redistribution (Lander, 1971; Murphy, 1971) is recognized (Cairns and McBreen, 1978) as perhaps the most serious life-limiting process associated with the secondary alkaline zinc electrode.

Investigators have identified several mechanisms by which zinc active-material redistribution might take place in a quiescent secondary cell:

(i) Electroosmotic forces can induce the flow of electrolyte, which results in convective transport of soluble zinc-bearing species (Choi et al, 1976).

(ii) Non-uniform current density distribution leads to concentration gradients, which result in the diffusion of soluble zinc-bearing species (McBreen, 1972).

(iii) Preferential nucleation of zinc onto zinc (rather than onto the electrode current-collector substrate) and cathodic H_2 evolution at the electrode edges can result in non-uniform zinc deposition during charge (Januszkiewicz et al, 1981).

(iv) Autocatalytic dissolution of zinc via $Zn(OH)_4^{-2}$ ions leads to an accelerated zinc dissolution rate near the electrode edges, where the $Zn(OH)_4^{-2}$ concentration tends to be higher (McKubre, 1983).

(v) Isolated zinc fragments can migrate across the electrode under the influence of potential gradients (Szpak et al, 1980).

Models (i) and (ii) suggest that the rate of zinc-material redistribution is strongly dependent upon the solubility of zinc-bearing species in the electrolyte. Model (iii) would predict that the zinc redistribution rate is strongly affected by the choice of current-collector material.

The purpose of the present work is to evaluate electrolytes that exhibit reduced zinc-species solubility for their ability to slow the rate of zinc redistribution and maintain the high performance that is characteristic of the secondary alkaline zinc electrode. According to models (i) and (ii) listed above, this should be possible, so long as the positive electrode is not adversely affected by the choice of

electrolyte. The goal of this project, and related work in this laboratory, is to characterize new components and materials that may improve the cycle-life performance of advanced secondary cells.

SOLUBILITY OF ZINC SPECIES IN ALKALINE ELECTROLYTE

The aqueous hydroxyl group forms complexes with Zn^{2+} for which the coefficients of complex formation have been reported (Reichle et al, 1975; Gubeli and Ste-Marie, 1967). Solubility products for zinc hydroxide have also been reported (Reichle et al, 1975; Pourbaix, 1974). From this information one can predict the solubility of zinc hydroxide in concentrated KOH; and given the solubility products between zinc and other anions, the effect of these anions on the solubility of oxidized zinc can, in principle, be determined. The situation is complicated, however, by the appearance of several crystalline and non-crystalline $Zn(OH)_2$ and ZnO precipitates that can form from zinc-containing alkaline solutions (Reichle et al, 1975; Pourbaix, 1974).

Zinc hydroxide is considered to be a sparingly-soluble salt, and its solubility product has been reported (Reichle et al, 1975) to vary from 10^{-13} to 10^{-21}, but the "best" value for ε-$Zn(OH)_2$ is reported as 3.5 x 10^{-17} for the following expression:

$$K_{sp} = (Zn^{2+})(OH^{-})^2 \tag{1}$$

Equation (1) is written in terms of activities, and K_{sp} is defined as the thermodynamic equilibrium constant, because the concentrations were measured in dilute solutions where the activity coefficients are nearly unity.

At high hydroxyl-ion concentrations the hydroxyl group is believed (Reichle et al, 1975; Gubeli and Ste-Marie, 1967; Dirkse, 1981) to

tetrahedrally complex the Zn^{2+} ion, and the overall complex-formation reaction has the following equilibrium expression:

$$\beta_4 = \frac{[Zn(OH)_4^{=}]\ \gamma_{Zn(OH)_4^{=}}}{[Zn^{2+}]\ [OH^-]^4\ \gamma^4_{OH^-}\gamma_{Zn^{2+}}} \qquad (2)$$

The complex-formation constant β_4 has been reported as 2×10^{12} to 5×10^{17}, and an average value of 2.7×10^{15} will be used in the calculations to follow. Combining equations (1) and (2) with a charge balance eliminates $[OH^-]$ and $[Zn^{2+}]$ from the equations to give the zinc tetrahydroxyl concentration in terms of the metal-ion concentration $M = [M^+]$, the activity coefficients γ, β_4 and K_{sp}:

$$[Zn(OH)_4^{=}] = \frac{M + X/4}{2} - 1/2\sqrt{\frac{X^2}{16} + \frac{MX}{2}} \qquad (3)$$

where

$$X = \frac{\gamma_{Zn(OH)_4^{=}}}{(\gamma_{OH^-})^2} \times \frac{1}{\beta_4 K_{sp}}$$

By comparing (Nichols, 1983) the complex-formation constants of the Zn mono-, di- and trihydroxides, it can be determined that the predominant species in concentrated (>1M) hydroxide solutions is $Zn(OH)_4^{=}$, so equation (3) provides a prediction of total soluble monomeric zinc in a

$Zn(OH)_2$-saturated alkaline solution.

Dimers or polymeric forms of tetrahedrally complexed Zn^{2+} have been proposed (Dirkse, 1981), but because of the effects of ionic strength on activity, the existence of these polymeric species cannot be predicted using Eq. (3).

Figure 1 shows the $Zn(OH)_2$ solubility predicted from equation (3), with all activity coefficients set equal to unity, compared to the experimentally-measured $Zn(OH)_2$ solubility. The predicted values show only fair agreement with measured values, and the discrepancies result from the use of unit activity coefficients, the uncertainty associated with the large variation in reported solubility products and complex-formation constants, and the use of dilute-solution equilibrium constants in the concentrated-electrolyte region. The lack of quantitative agreement between predicted and measured $Zn(OH)_2$ solubilities suggests that one should not have great confidence in subsequent predictions of the effect of various anions on the solubility of oxidized zinc species. Such computations would introduce yet another poorly-known quantity, i.e., the solubility product between zinc and the other anions.

The solubility of ZnO in aqueous KOH electrolyte (Dyson et al, 1968; Dirkse, 1959; Falk and Salkind, 1969) is only 30-37% of that of $Zn(OH)_2$. It is this lower ZnO solubility that determines the equilibrium concentration of Zn species in concentrated alkaline solutions. When $Zn(OH)_2$ is dissolved in alkaline solutions, the Zn^{2+} concentration and all other zinc hydroxyl-ion complex species are higher than their equilibrium concentrations with ZnO. Therefore the $Zn(OH)_2$-saturated solution is

unstable and ZnO will precipitate, though slowly (Dirkse, 1981).

It has been reported (Dalin et al, 1964) that the zinc redistribution rate is reduced when the hydroxide concentration is reduced, although these observations were made at concentrations higher than 31 wt% KOH. KOH concentrations lower than 31 wt% have not been used because of lower utilization of the $Ni(OH)_2$ in the nickel-oxide counter electrode (Falk and Salkind, 1969), and because of reduced conductivity. Another potential problem for Zn electrodes discharged in electrolytes with lower hydroxide-ion concentration is a possible increased tendency toward passivation.

To reduce the zinc species concentration in KOH electrolyte, several modified electrolytes have been used, but none have been found to give reduced solubility, high conductivity, and high counter-electrode utilization at the same time. At low hydroxide-ion concentration, fluoride, phosphate, borate and oxalate ions (Thorton and Carlson, 1980; Cenek et al, 1977; Schneider et al, 1973; U.S. Patents, 1980, 1981 and 1974; Japanese Patent, 1975) have been tested for various proposed advantages.

Borate- and fluoride-containing electrolytes with a low KOH concentration were chosen for the experiments reported here. Figure 2 shows the ZnO solubility in some of these combinations as a function of the hydroxide-ion concentration of the initial electrolyte. It is obvious for the electrolytes shown that the added anion has no significant affect on the ZnO solubility. The solubility appears to be determined solely by the hydroxide-ion concentration. The alkalinity of the borate-containing electrolyte is unknown, but the range of possible hydroxide concentrations includes the hydroxide concentration of a KOH

electrolyte with the same ZnO solubility. No attempt has been made here to calculate the free hydroxyl-ion concentration in the borate-containing electrolytes using boric-acid dissociation constants.

The electrolytes used in this work are listed in Table I, and they were chosen to have a zinc-species solubility approximately one-fourth of that in standard alkaline electrolyte, which is also listed.

Table I

Electrolyte Compositions[a]

Standard:	30% KOH, 1% LiOH (7.4M OH^-), ZnO saturated
Low KOH:	14.4% KOH, 1.12% LiOH (3.5M OH^-), ZnO saturated
Alkaline-fluoride:	15.3% KOH (3.5M OH^-), 15.0% KF, ZnO saturated, LiF saturated
Alkaline-borate:	21.5% K_3BO_3, 1.13% Li_3BO_3, (1.7M BO_3^{3-}), ZnO saturated

---

a The wt% and molarities shown in the table are the compositions before addition of ZnO to the electrolyte.

EXPERIMENTAL

Electrode Specifications - The zinc electrodes were fabricated using a filter-table method (Nichols, 1983). A mixture of ZnO* (96 wt%), polytetrafluoroethylene** (4 wt%) and PbO* (2 wt%) were blended*** with H_2O, and the resulting slurry was vacuum-filtered to produce a filter cake. The purpose of the PTFE additive is to impart strength to the finished electrode, and the PbO additive is intended to suppress unwanted H_2 evolution from the zinc electrode. A 62-mm tall and 70-mm wide (dimensions chosen to match those of the positive electrodes) Cu screen+, onto which a 0.25mm thick, 1cm-wide Cu tab had been spot-welded, was electroplated with Pb from a lead fluoroborate solution to form a 13μm Pb layer. The screen was then placed between two filter cakes, and the electrode was pressed at 13.4 kN, using spacers of appropriate thicknesses, to a thickness of 0.82mm ± 0.03mm. Its final porosity (on a metal basis) was 76.2% ± 0.5%. Sufficient ZnO (6.1g ± 0.1g) was used to provide a theoretical capacity of 4.05 Ah ± 0.05 Ah, which is 3.0 times that of the positive electrodes.

The sintered nickel positive electrodes++ were fabricated using a proprietary process. A $Ni(OH)_2$ loading of 56-57 mg/cm^2 was used, and two nickel electrodes were loaded into each cell to provide a cell

---

* Mallinckrodt, Inc., Paris, KY, 99.9% pure.

** E.I. Dupont de Nemours and Co., Wilmington, DE, Teflon Type 30 dispersion.

*** Sears, Roebuck Company 7-speed blender, no. 5 setting.

\+ Exmet Corp., Bridgeport, CT, mesh 3 Cu 6-4/0.

++ Eagle-Picher Industries, Inc., Colorado Springs, CO.

capacity of 1.35 Ah. A 0.13mm-thick, 1cm-wide Ni tab was spot-welded onto each nickel electrode, as was a Ni wire (to permit overpotential measurements free of the ohmic potential drop in the tab).

Separator and Wick - Three layers of Celgard* 3401 microporous polypropylene sheet were heat-sealed around the Zn electrode. The two inner layers were sealed together and trimmed, and the outer layer was then sealed around the first two. Wicking material was used to help avoid drying of the NiOOH electrode. Non-woven nylon material, Pellon 2502K4,** was wrapped around each NiOOH electrode.

Electrolyte Preparation - Electrolytes, the compositions of which are listed in Table I, were made up and stored in polyethylene bottles connected to a scrubber to prevent CO_2 ingress. Potassium hydroxide+ was obtained as a 46.3 wt% solution containing $\leq$0.04 wt% K_2CO_3, and the LiOH purity++ was 98%. The KF • $2H_2O$ used+++ contained $\leq$0.01 wt% K_2CO_3, and the H_3BO_3 was of ACS reagent-grade purity.+ Deionized 15 MΩ-cm H_2O was used.

Following preparation of each solution, reagent-grade ZnO was added in sufficient quantity to saturate the electrolyte. The slurry was then stirred for at least 5 days at room temperature (18°C - 28°C). Densities were determined by weighing a volume of electrolyte from a 20mL

---

* Celanese Fibers Corp., Summitt, NJ.

** Pellon Corp., Chelmsford, MA.

\+ J.T. Baker Chemicals Co., Phillipsburg, NJ.

++ Matheson, Coleman and Bell Manufacturing Chemists, Norwood, OH.

+++ Malinckrodt, Inc., Paris, KY.

burette, which gave a ±0.25% accuracy, or a 0.25mL burette, which gave a ±0.4% accuracy.

Cell Design - The cell parts were machined from acrylic sheet and rod. An exploded view of a typical cell is shown in Fig. 3. The two end sheets were machined flat to within 0.03mm and were separated by a 6.60mm-thick frame-shaped spacer, which was machined flat to within 0.05mm. The inner dimensions of the spacer were 1.5mm larger than those of the electrodes on each side and the bottom.

One face of the cell case contained a 0.5mm-diameter capillary, and was drilled and tapped at that location to permit attachment of the reference-electrode compartment. This compartment consisted of a 4.7mm-diameter column containing an Hg/HgO reference electrode, a fill port, and a 0.86mm-diameter, 3.2cm-long capillary, all of which were machined from a single acrylic rod. A Pt wire passed through the lower portion of the column to provide electrical contact to the Hg without touching the electrolyte. The reference-electrode compartment is visible in the view of a fully assembled cell shown in Fig. 4.

The materials for the other cell parts were chosen on the basis of their resistance to chemical attack by strongly alkaline solutions. Carbon-filled ethylene-propylene "O"-rings, polyethylene and acrylic packing materials, a nylon filling plug, and nickel or 300-series stainless-steel fill tubing were used.

Cell Assembly - Prior to assembling the cell, all parts were washed with detergent, rinsed with water, and then rinsed with 5% reagent-grade acetic-acid solution to remove any residual carbonate compounds.

The packing tightness of the electrode stack is determined by the thickness of the frame-shaped spacer and the polyethylene packing sheets. The packing thickness was chosen so that the electrode assembly (Zn electrode, separator, wick, and NiOOH electrodes) received the same compression as that produced by a pressure of 27.6 kN/m^2. This resulted in the Pellon wick being compressed to 0.15mm thickness.

Polyethylene packing sheets were cut to the exact dimension of the inner width of the cell and at least 1cm higher than the electrode (to minimize any extra electrolyte reservoir above the electrodes). In order to prevent gas from blocking the capillary that connects the reference-electrode compartment to the cell, the 0.5mm-diameter capillary was packed with an acrylic yarn.

Next, the cell was assembled and leak-checked under vacuum. The reference-electrode compartment was filled with Hg and HgO, and the cell was weighed. The cell was evacuated again and filled with electrolyte to above the polyethylene packing sheets. The cell was then reweighed and allowed to stand for at least 24 hours to permit electrolyte to soak into the electrode pores. The cell was vented to a 1M NaOH gas scrubber, through which air was passed at approximately 500mL/min. This arrangement was necessary to prevent CO_2 ingress and subsequent formation of K_2CO_3 in the electrolyte.

<u>NiOOH Electrode Formation</u> - For the first few cycles ("formation cycles"), the cell was charged for 20 hours at a rate sufficient to fully charge the NiOOH electrode in 10 hours. The cell was then discharged at a rate sufficient to fully discharge the NiOOH electrode in 2.5 hours until H_2 evolved from the NiOOH electrode, at which time

the discharge rate was lowered by a factor of 4 and continued until the cell potential reached 0.0 volts. This was then repeated twice, followed by a 20-hour charge, after which time regular cycling could begin. These formation cycles also established the molar ratio of Zn/ZnO at 2/1 for the fully charged cell at the beginning of regular cycling. Because a 3/1 Zn/NiOOH stoichiometric ratio is used, the molar ratio of Zn/ZnO ranges from 2/1 (fully charged) to 1/2 (fully discharged) as the cell is cycled, so long as the charging and discharging processes are 100% efficient.

Life-cycle Testing - The cells were cycled under controlled charge and discharge regimes using a combination of analog and digital equipment, which is fully described elsewhere (Katz et al, 1983). Cell current was maintained at a digitally-set level to within ±0.25mA and monitored to an accuracy of ±1mA. The cell and electrode potentials were measured to an accuracy of ±2mV.

Cells were charged at 225mA constant current for 6 hours or until passing 104% of the coulombs discharged on the previous half-cycle. The 4% overcharge is necessary to accommodate the inefficiency (O_2 evolution) of the NiOOH during charging. Cells were discharged at 540mA constant current for 2.5 hours (which corresponds to the 1.35Ah cell capacity) or until the cell potential dropped to 1.1 volts. An open-circuit "rest time" of 10 minutes occurred at the end of each half-cycle.

The cells were cycled for 125 cycles, or until the capacity fell to less than 60% of the design capacity, or until the cell shorted. From time to time (typically every 20-50 cycles), a rise in Zn-electrode overpotential near the end of charge was observed, which indicates a

depletion of available ZnO. When this condition occurred, it was necessary to completely discharge the cell to 0.0 volts, which resulted in complete conversion of all available metallic Zn to ZnO. Next, a formation half-cycle was performed, which provided an appropriate molar ratio of Zn/ZnO.

Post-Cycling Tests - At the end of cycle-life testing, the zinc electrodes were examined to determine extent of the zinc redistribution, state of charge, existence of dendritic penetration through the separator, and the quantity of electrochemically-inactive zinc. In addition, portions of the zinc electrodes were examined by Scanning Electron Microscopy (SEM).*

The extent of zinc redistribution on each negative electrode was determined by obtaining an X-ray image** of the electrode both before and after cycling. The state of charge of the negative electrode (the Ah of electrochemically-active zinc remaining in the cell after the last discharge or charge) was determined by discharging the electrode in excess electrolyte with the separator removed.

The electrode was then immersed in HCl and the quantity of H_2 produced was measured. Because HCl will not produce hydrogen from other materials in the electrode (Cu, Pb, ZnO), the H_2 evolved is a direct result of the dissolution of zinc metal, and is therefore a measure of the quantity of electrochemically-inactive Zn.

---

* Advanced Materials Research Corp.

** Profax Co.

In order to examine the zinc-electrode morphology, it was necessary to bisect the electrodes and set aside half of each electrode for SEM analysis. For the cells that were disassembled in the discharged condition, the zinc electrode was bisected after determining the state of charge, as shown in Fig. 5. For the cells that were disassembled in the charged condition, the zinc electrode was bisected after obtaining an X-ray of the electrode, as shown in Fig. 6. Because the zinc material redistribution process cannot be expected to produce a perfectly symmetrical electrode, errors can be expected when results (e.g., Ah of Zn) of tests performed on half of an electrode are doubled to characterize the entire electrode.

RESULTS AND DISCUSSION

Electrical Performance - A total of 8 cells were subjected to cycle-life testing to evaluate the 4 electrolytes listed in Table I. Two cells contained standard electrolyte, two cells contained low KOH electrolyte, two cells contained alkaline-fluoride electrolyte, and two cells contained alkaline-borate electrolyte. Each identical pair of cells was cycled electrically in series, and computer-implemented decisions to terminate charge or discharge during any given half-cycle were based on the voltage behavior of the cell exhibiting the lower capacity: e.g., discharge was ended as soon as the potential of either cell dropped to 1.1 volts. This configuration created no particular problems, so long as the capacity of each cell cycled in series remained closely matched.

Figures 7-10 show potential vs. time behavior for 5 of the 8 cells cycled. In general, the zinc electrode displays low overpotentials,

both on charge and on discharge, and the NiOOH electrode limits the cell discharge capacity.

An example of the results of a slight capacity mis-match between two cells cycled in series can be seen by comparing Figs. 9a and 9b. Both cells contained alkaline-fluoride electrolyte, but the cell shown in Fig. 9b has a capacity larger than that of the cell shown in Fig. 9a, so the cell in Fig. 9b was never fully discharged (the cell voltages shown on the right-hand side of Fig. 9b never drop to 1.1 volts). Also, in Fig. 9b, voltages and zinc-electrode potentials show that the zinc electrode exhibited large overpotentials near the end of charge after cycle 100. This behavior is indicative of insufficient ZnO available to support the charging process.

The cell capacities are plotted as a function of cycle number in Fig. 11. Because each pair of cells having the same electrolyte was cycled in series, the capacity behavior is the same for each electrolyte. The discontinuities are artifacts caused by the periodic need to re-establish the appropriate Zn/ZnO balance, as described previously. The cell with standard electrolyte shows a rapid capacity decline after cycle 110. The other cells show a more stable capacity, but the initial capacities of the cells containing alkaline-fluoride and low KOH electrolytes are about 10% lower than the 1.35Ah design capacity, and the alkaline-borate also showed a reduced capacity during most of its life. This somewhat reduced capacity, when compared to that of the cells containing standard electrolyte, could be caused by the lower electrolyte conductivity and/or a reduction in NiOOH electrode capacity as a result of low hydroxyl-ion concentration. In addition, the cells using

alkaline-fluoride electrolyte may have had a reduced capacity because LiOH, which is added to alkaline electrolytes to benefit the NiOOH-electrode performance, is nearly insoluble in aqueous KOH-KF mixtures due to precipitation of LiF.

Both of the cells cycled in standard electrolyte shorted: one (prematurely) at cycle 26 and the other at cycle 118.

Zinc Redistribution - The zinc distribution, before and after cycling, is shown in Figs. 12-15 for cells cycled in each of the four electrolytes. The zinc redistribution patterns were very similar for each identical cell pair.

The zinc electrodes cycled in low KOH electrolyte exhibited a typical (McBreen, 1972; Lander, 1971; Poa and Wu, 1978) zinc material redistribution pattern, as shown in Fig. 12, but the zinc redistribution pattern observed in cells cycled with standard electrolyte (Fig. 13) and alkaline-borate electrolyte (Fig. 14) showed a pattern opposite from that expected. This unusual pattern was repeatable (as stated above, for each electrolyte identical cell pairs were cycled), and a similar pattern of zinc redistribution has been observed on another zinc electrode cycled in standard electrolyte.* None of the models of zinc active-material redistribution appears to predict a dramatic change in direction of zinc migration as the KOH concentration is varied. The zinc redistribution pattern on electrodes cycled in alkaline-fluoride electrolyte was of the expected form and showed the least amount of redistribution among the electrolytes tested.

---

* To be published.

The ratio of cell capacity retained to zinc-electrode area retained is listed in Table II. It is seen that in standard electrolyte the cell capacity is less sensitive to the extent of Zn area loss. For the low-hydroxyl-ion concentration electrolyes, there is a direct relationship between zinc electrode area retained and cell capacity retention.

Also listed in Table II are the average percent depths of discharge for the various cells. Because of the lower capacity of the NiOOH electrodes, the cells cycled in the low hydroxyl-ion-concentration electrolytes were subjected to an average depth of discharge lower than that for the cell using standard electrolyte, which was cycled to an average of 93% of the nominal 1.35Ah capacity. Within the range studied, there appears to be no clear link between the average depth of discharge and the extent of zinc material redistribution.

Table II

Cell Capacity Retention

Electrolyte	Area Loss (%)	Ratio of initial capacity retained to zinc-electrode area retained (Ah/%)	Average Depth of Discharge (%)
Standard	56	1.50	93.0
Low KOH	36, 39	1.01, 1.06	76.2
Alkaline-fluoride	13, 18	0.88, 0.94	82.5
Alkaline-borate	11, 14	0.82, 0.84	88.8

Electrolyte Measurements - The solubility of ZnO in each of the four electrolytes was measured, and the results are listed in Table III. These data compare favorably to the solubilities measured in other

laboratories, which are plotted in Fig. 2, although the value for the low KOH electrolyte appears to be slightly higher than comparable values obtained by Dirkse (1959). Measured densities are also listed in Table III.

After cycling, the cells were placed on open-circuit for about two hours, after which time the cell potentials reached steady values. A syringe was then used to draw a sample of electrolyte from the top of the cell compartment outside of the separator. The density and zinc content of each sample was measured, and it was determined that the Zn concentration in each electrolyte fell within +25%/-31% of the saturation values listed in Table III. This result verifies that the low KOH, alkaline-fluoride, and alkaline-borate electrolytes successfully reduce the zinc-species concentration in operating Zn/NiOOH cells, and that conditions leading to highly supersaturated electrolytes were not attained under the cycling regimes used in this study.

Table III

ZnO Solubility and Electrolyte Density
at 21±1°C unless otherwise noted

Electrolyte	Zn content (mg Zn/mL), ±1.5% accuracy	Density (g/mL)
Standard	50.8	1.339±0.4%
Low KOH	16.0	1.156±0.4%
Alkaline-fluoride[a]	0	1.284±0.4%
Alkaline-fluoride	12.6	1.328±0.4%
Alkaline-borate[b]	0	1.251±0.25%
Alkaline-borate	14.4	1.265±0.4%

a) At 23±1°C, no ZnO
b) At 25±1°C, no ZnO

Zinc Penetration through the Separator - After each cell was disassembled, the separator and wick were examined for evidence of zinc material, and the following observations were made:

(i) Both cells containing standard electrolyte shorted. The cell disassembled in the charged condition after 34 cycles showed a 1mm-diameter zinc growth that had penetrated the separator and wick and was attached to the NiOOH electrode. The cell disassembled in the discharged condition after 118 cycles contained some zinc in both the separator and wick.

(ii) Both cells containing low KOH electrolyte showed a small amount of zinc outside of the separator, and the cell disassembled in the charged condition showed some zinc on the wick.

(iii) No zinc was observed in the separator or wick of the cells cycled in the alkaline-fluoride electrolyte.

(iv) In cells cycled in alkaline-borate electrolytes, no zinc was found in the wick, and a small amount of zinc was found in the lower corners of the separator (probably caused by a defective separator seal).

It is seen that the cells which showed the greatest zinc-electrode area retention also showed the greatest resistance to penetration of the separator by zinc dendrites. This observation points to a correlation between zinc-electrode charging current density (based on the remaining area of the zinc electrode) at the end of cycling and the extent of dendritic penetration through the separator. However, zinc dendrite growth has been correlated (Diggle et. al, 1969) not with current density, but with electrode overpotential, where dendrites are expected at overpotentials greater than 75mV in 10 wt% KOH. The present experiments show no correlation between dendrite penetration through the separator and Zn electrode overpotential; Fig. 9b shows large (>100mV) overpotentials on the zinc electrode during charge, yet no dendrites were observed, whereas Fig. 7 shows only modest (<50mV) overpotentials on the zinc electrode during charge, yet the cell shorted due to zinc dendrite penetration through the separator.

Zinc Material Balance - The quantity of electrochemically-inactive (isolated or passivated) zinc was determined in the tab-containing half of the vertically bisected electrode. Measured quantities ranged from zero to a maximum of 2% of the initial zinc contained in the electrode half.

Table IV lists the zinc material-balance data for cells disassembled in the discharged state. The zinc material balance for the cell cycled in standard electrolyte is suspect because this cell developed a short. For the cell cycled in low-KOH electrolyte, there was 0.55Ah (1.39-0.84) of metallic zinc available at the end of discharge, which was apparently sufficient to prevent large overpotentials on the zinc electrode (see Fig. 8). For the cells cycled in alkaline-fluoride and alkaline-borate electrolytes, there were 0.45Ah and 0.58Ah, respectively, of metallic zinc available at the end of discharge. Figure 9a shows significant overpotentials on the zinc electrode at the end of discharge for the cell cycled in alkaline-fluoride electrolyte, and Fig. 10 shows similar behavior for the cell cycled in alkaline-borate electrolyte. This observation suggests that the alkaline-fluoride and alkaline-borate electrolytes require more Zn metal (than that required by an electrode cycled in pure alkaline electrolyte) to avoid excessive overpotentials on discharge. Similarly, the cell cycled in alkaline-borate electrolyte contained 1.75Ah of ZnO at full charge, and Fig. 10 shows significant overpotentials on the Zn electrode near the end of charge, which suggests that the alkaline-borate electrolyte requires more ZnO (than that required by an electrode cycled in pure alkaline electrolyte) to avoid excessive overpotentials on charge.* This phenomenon could be caused by a slow ZnO dissolution rate in this electrolyte.

---

* The electrode cycled in alkaline-fluoride electrolyte contained 2.01Ah of ZnO at full charge, which was sufficient to avoid substantial overpotentials (Fig. 9a).

Table IV

Zinc Charge and Material Balances for Electrodes from Cells Disassembled in the Discharged State

Electrolyte	Initial Zn metal basis, Ah (gm)	Final Cell Capacity, Ah	Final Zinc metal, Ah	ZnO at full charge, Ah	Lost Zn metal basis, gm
Standard	4.03 (4.91)	0.73	1.15[a]	—	1.28[b]
Low KOH	4.10 (4.99)	0.84	1.39	71.18	1.86[b]
Alkaline-Fluoride	4.03 (4.91)	0.93	1.38	2.01	0.77
Alkaline-Borate	4.02 (4.90)	1.0	1.58	1.75	0.84

a Possible error due to short

b Some loss of material during washing procedure

Zinc charge and material balance data for electrodes from cells disassembled in the charged state are listed in Table V. As for the cells disassembled in the discharged state, a substantial amount of the zinc cannot be accounted for by analysis of the electrodes. The material balance did not account for the amount of zinc in the electrolyte (not in the electrodes) in excess of saturation, but the degree of supersaturation was small, so very little error is expected by this omission. Also not accounted for was the amount of supersaturated electrolyte within the pores of the electrode. An upper bound on this quantity can be obtained by using the supersaturated concentrations measured by Dirkse (1970): 10% for 7.4M KOH and 5% for 3.5M KOH; and the 76% porosity of the zinc electrode. The possible Zn content ranges from 0.15 to 0.40 gm, which is too small to account for the 0.77-2.44 gm of unaccounted-for zinc. It is likely (Seiger, 1981) that the missing zinc accumulated in the NiOOH electrodes.

Zinc Electrode Morphology - Samples of charged and discharged electrodes were examined by SEM. In all cases, the predominant structure was highly porous (Fig. 16b), except for an isolated area found on a zinc electrode taken from a cell cycled in low KOH electrolyte that was disassembled in the charged state (Figs. 16a and 17).

Table V

Zinc Charge and Material Balances for Electrodes from Cells Disassembled in the Charged State

Electrolyte	Initial Zn metal basis, Ah (gm)	Final Zn in half of electrode, Ah (gm)	Lost Zn metal basis, (gm)
Standard	4.00 (4.88)	0.11 (0.13)*	2.44
Low KOH	3.94 (4.81)	0.55 (0.67)	2.07
Alkaline-Fluoride	4.10 (5.00)	1.45 (1.76)	1.10
Alkaline-Borate	4.08 (4.98)	1.09 (1.33)	1.64

* shorted

CONCLUSIONS

Electrolytes exhibiting reduced ZnO solubility were shown to reduce the rate of zinc material redistribution in 1.35Ah Zn/NiOOH cells. Alkaline-fluoride and alkaline-borate electrolytes reduced the rate of loss of zinc area from 0.46%/cycle to 0.09-0.14%/cycle, when compared to standard electrolyte. In addition, the alkaline-fluoride and alkaline-borate electrolytes eliminated dendritic zinc growth through the separator, even with zinc-electrode overpotentials as high as 290mV. These electrolytes also maintained a highly porous electrode structure, and less than 2% of the zinc remaining after cycling was electrochemically inactive.

Cell electrical performance data showed that the NiOOH electrode limited cell capacity throughout the life of all cells tested. For the cells using electrolytes having reduced ZnO solubility, the ratio of cell capacity retained to zinc-electrode area retained was nearly constant, which suggests that the capacity losses of the NiOOH electrodes, and the cells, were caused by a reduction in local NiOOH-electrode capacity opposite areas on the zinc electrode that were devoid of active material.

Cells cycled in electrolytes having reduced ZnO solubility showed an initial capacity about 10% lower than those cycled in standard electrolyte. Cells cycled in alkaline-fluoride and alkaline-borate electrolytes were more likely to show significant (i.e., >30mV) overpotentials near the end of charge or discharge, when compared to cells cycled in pure alkaline electrolyte with equal amounts of available active material.

ACKNOWLEDGEMENT

This work was supported by the Assistant Secretary for Conservation and Renewable Energy, Office of Energy Systems Research, Energy Storage Division of the U.S. Department of Energy under Contract No. DE-AC03-76SF00098.

NOMENCLATURE

K_{sp}	Solubility product
M	Metal-ion concentration, mol/liter
X	Parameter in Eq. (3)
β	Complex-formation constant
γ	Activity coefficient

REFERENCES

Brown, H.E., "Zinc Oxide," The New Jersey Zinc Co., New York (1957).

Cairns, E.J. and McBreen, J., in Advances in Electrochemistry and Electrochemical Engineering, Vol. 11, H. Gerisher and C.W. Tobias, Eds., John Wiley and Sons, New York (1978).

Cenek, M., Kouril, O., Sandera, J., Touskova, A. and Calabek, M., in Proc. 10th Int. Power Sources Symp., Power Sources 6, D.H. Collins, Ed., Academic Press, New York, p. 215 (1977).

Choi, K.W., Bennion, D.N. and Newman, J., J. Electrochem. Soc. 123, 1616 (1976).

Dalin, G.A., Sulkes, M. and Stachurski, Z., in Proc. 18th Annual Power Sources Conf., PSC Publications Committee, Atlantic City, NJ (1964).

Diggle, J.W., Despic, A.R. and Bockris, J. O'M., J. Electrochem. Soc. 116, 1503 (1969).

Dirkse, T.P., J. Electrochem. Soc. 128, 1412 (1981).

Dirkse, T.P., J. Electrochem. Soc. 106, 154 (1959).

Dirkse, T.P., in "Power Sources 3, Proc. of 7th Int. Symp.," D.H. Collins, Ed., Oriel Press, Newcastle-Upon-Tyne, England (1970).

Dyson, W., Schreier, L., Sholette, W. and Salkind, A., J. Electrochem. Soc. 115, 566 (1968).

Falk, S.U. and Salkind, A.J., "Alkaline Storage Batteries," John Wiley and Sons, New York, p. 586 (1969).

Gubeli, A.O. and Ste-Marie, J., Can. J. Chem. 45, 827 (1967).

Januszkiewicz, S., Vaidyanathan, H., Dodin, M. and Leo, T., "Annual Report for 1980 on Research, Development and Demonstration of Nickel-Zinc Batteries for Electric Vehicle Propulsion," Argonne National Laboratory Report No. ANL/OEPM-80-13 (1981).

Japanese Patent 26,004 (March 18, 1975).

Katz, M.H., Nichols, J.T., McLarnon, F.R., Cairns, E.J. and Katz, J.E., J. Power Sources 10, 149 (1983).

Lander, J.J., in Zinc-Silver Oxide Batteries, A. Fleisher and J.J. Lander, Eds., John Wiley and Sons, New York (1971).

McBreen, J., J. Electrochem. Soc. 119, 1620 (1972).

McKubre, M.C.H., "Temperature Limitation of Primary and Secondary Alkaline Battery Electrodes," Lawrence Berkeley Laboratory Report No. LBL-16141 (1983).

Murphy, J.J., Chem. Technol. 1, 487 (1971).

Nichols, J.T., "Active Material Redistribution Rates in Zinc Electrodes: Effect of Alkaline Electrolyte Compositions Having Reduced Zinc Oxide Solubility," M.S. Thesis, University of California Report No. LBL-17397 (1983).

Poa, S.P. and Wu, C.H., J. Appl. Electrochem. 8, 427 (1978).

Pourbaix, M., "Atlas of Electrochemical Equilibrium in Aqueous Solutions," French portions translated by J.A. Franklin, 2nd Eng. Edition, Nat. Assoc. of Corr. Eng., Houston, TX (1974).

Reichle, R.A., McCurdy, K.G. and Hepler, L.G., Can. J. Chem. 53, 3841 (1975).

Schneider, F.A., "Power Sources 4, Proc. of 8th Int. Symp.," p. 115, D.H. Collins, Ed., Oriel Press, Newcastle-Upon-Tyne, England (1973).

Seiger, H.N., Proc. 16th Intersoc. Energy Conv. Eng. Conf., Vol 1, p. 102, ASME, New York (1981).

Szpak, S., Gabriel, C.J. and Katan, T., J. Electrochem. Soc. 127, 1063 (1980).

Thornton, R.F. and Carlson, E.J., J. Electrochem. Soc. 127, 1448 (1980).

U.S. Patent 4,224,391 (Sept. 23, 1980).

U.S. Patent 4,247,610 (Jan. 27, 1981).

U.S. Patent 3,849,199 (Nov. 19, 1974).

FIGURE CAPTIONS

Fig. 1. Comparison of $Zn(OH)_2$ solubility measured at 25°C by P.R. Mallory Co. (Falk and Salkind, 1969) with that calculated using Eq. (3).

Fig. 2. Solubility of ZnO in alkaline electrolytes with F^-, BO_3^{3-}, and PO_4^{3-} compared to solubility of ZnO in KOH electrolytes. Arrows for borate-containing electrolytes indicate possible range of free hydroxyl ion concentration.

● Dirkse (1959)

▲ ■ Thornton and Carlson (1980)

■ KOH

▲ Fluorides, phosphates and borates added

Fig. 3. Exploded view of cell case. A separator-wrapped Zn electrode is held between two NiOOH electrodes.

Fig. 4. Fully assembled cell. A separator-wrapped Zn electrode is held between two wick-wrapped NiOOH electrodes.

Fig. 5. Post-test analysis procedure for cells disassembled in the discharged condition.

Fig. 6. Post-test analysis procedure for cells disassembled in the charged condition.

Fig. 7. Cell voltage and electrode potentials for a cell cycled in standard electrolyte. The numbers refer to the cycle number.

Fig. 8. Cell and electrode potentials for a cell cycled in low KOH electrolyte. The numbers refer to the cycle number.

Fig. 9a. Cell and electrode potentials for a cell cycled in alkaline-fluoride electrolyte. The numbers refer to the cycle number.

Fig. 9b. Cell and electrode potentials for a cell cycled in alkaline-fluoride electrolyte. The numbers refer to the cycle number.

Fig. 10. Cell and electrode potentials for a cell cycled in alkaline-borate electrolyte. The numbers refer to the cycle number.

Fig. 11. Cell capacity vs. cycle number.

HighD: Standard electrolyte

LowA : Low KOH electrolyte

KFF : Alkaline-fluoride electrolyte

BO3H : Alkaline-borate electrolyte

Fig. 12. X-ray Image of Zinc Electrode Cycled in Low KOH Electrolyte. 1.35Ah design capacity electrode, with three times theoretical ZnO, cycled between two NiOOH counter electrodes at an average depth of discharge of 76.2% of design capacity in a 14.4% KOH-1.1% LiOH, ZnO-saturated electrolyte. The electrode is shown before cycling, and in the discharged state after cycle 124 with an estimated 36% loss of area. The magnification is 0.81, the X-ray energy was 60KeV and the dose was 100mAs.

Fig. 13. X-ray Image of Zinc Electrode Cycled in Standard Electrolyte. 1.35Ah design capacity electrode, with three times theoretical ZnO, cycled between two NiOOH counter electrodes at an average depth of discharge of 94.2% of design capacity in a 30% KOH-1% LiOH, ZnO-saturated electrolyte. The electrode is shown before cycling, and in the charged state on cycle 34 with an estimated 52% loss of area. The magnification is 0.84, the X-ray energy was 60KeV and the dose was 100mAs.

Fig. 14. X-ray Image of Zinc Electrode Cycled in Alkaline-Borate Electrolyte. 1.35Ah design capacity electrode, with three times theoretical ZnO, cycled between two NiOOH counter electrodes at an average depth of discharge of 88.8% of design capacity in a 21.5% K_3BO_3-1.13% Li_3BO_3,ZnO-saturated electrolyte. The electrode is shown before cycling, and in the discharged state after cycle 125 with an estimated 11% loss of area. The magnification is 0.80, the X-ray energy was 60KeV and the dose was 100mAs.

Fig. 15. X-ray Image of Zinc Electrode Cycled in Alkaline-Fluoride Electrolyte. 1.35Ah design capacity electrode, with three times theoretical ZnO, cycled between two NiOOH counter electrodes at an average depth of discharge of 82.5% of design capacity in a 15.3% KOH-15.0% KF, ZnO-saturated electrolyte. The electrode is shown before cycling, and in the discharged state after cycle 130 with an estimated 13% loss of area. The magnification is 0.81, the X-ray energy was 60KeV and the dose was 100mAs.

Fig. 16. Comparison of Morphology of Charged Electrode Low KOH. Cycled in 14.4% KOH-1.1% LiOH electrolyte for 124 cycles between two NiOOH counter electrodes at an initial charge current density of 2.6mA/cm^2. a) The location on the electrode is 0.8mm below the location shown at the center of Figure 17. b) The location is shown at the center of Figure 17.

Fig. 17. Low Magnification SEM of Compact Area on Electrode Low KOH. The electrode is cycled in 14.4%-1.1% LiOH electrolyte for 124 cycles between two NiOOH counter electrodes. Upper right of photograph is toward the electrode top and the upper left is toward the tab side of the electrode.

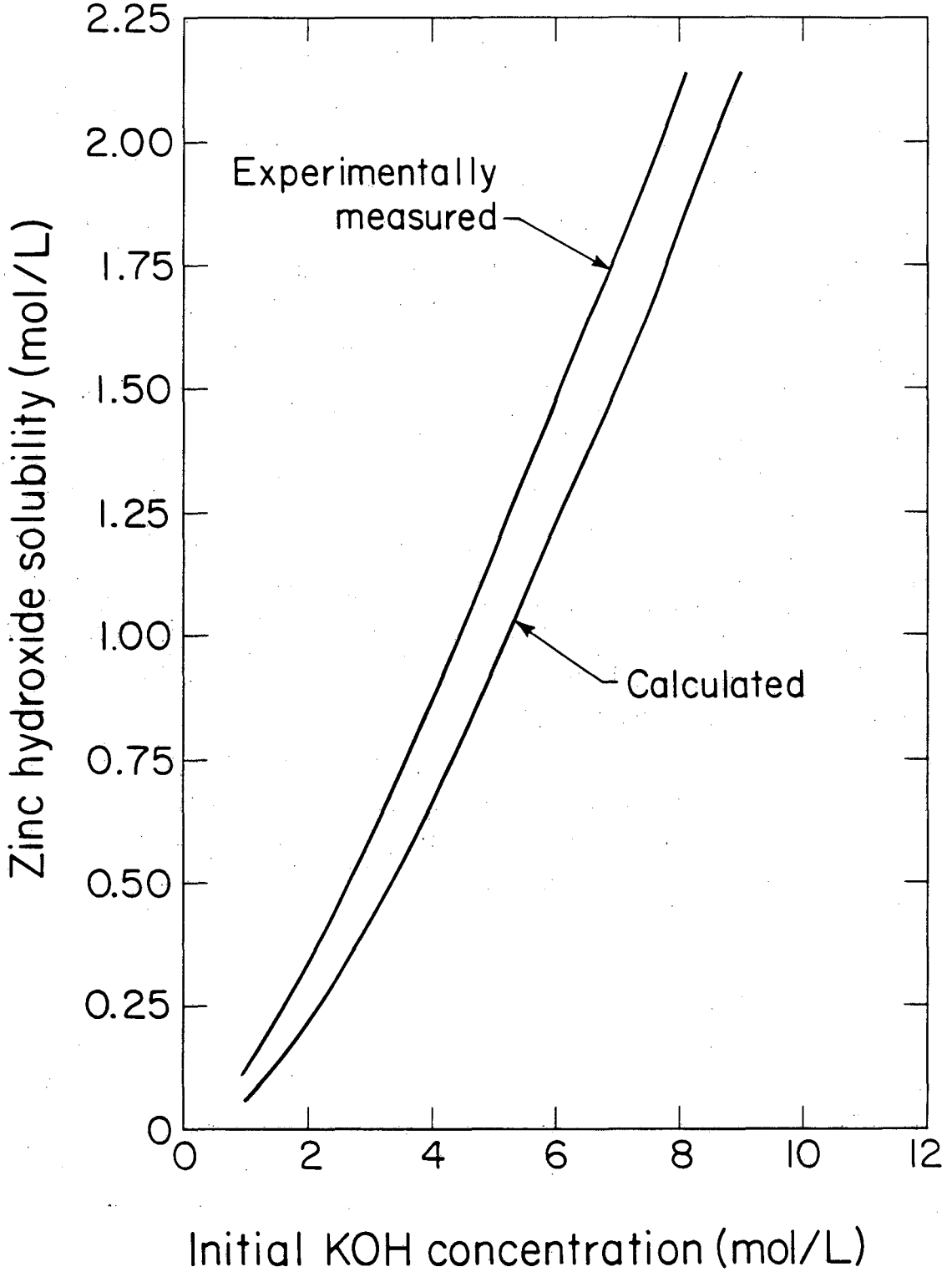

XBL 837-10683

Fig. 1

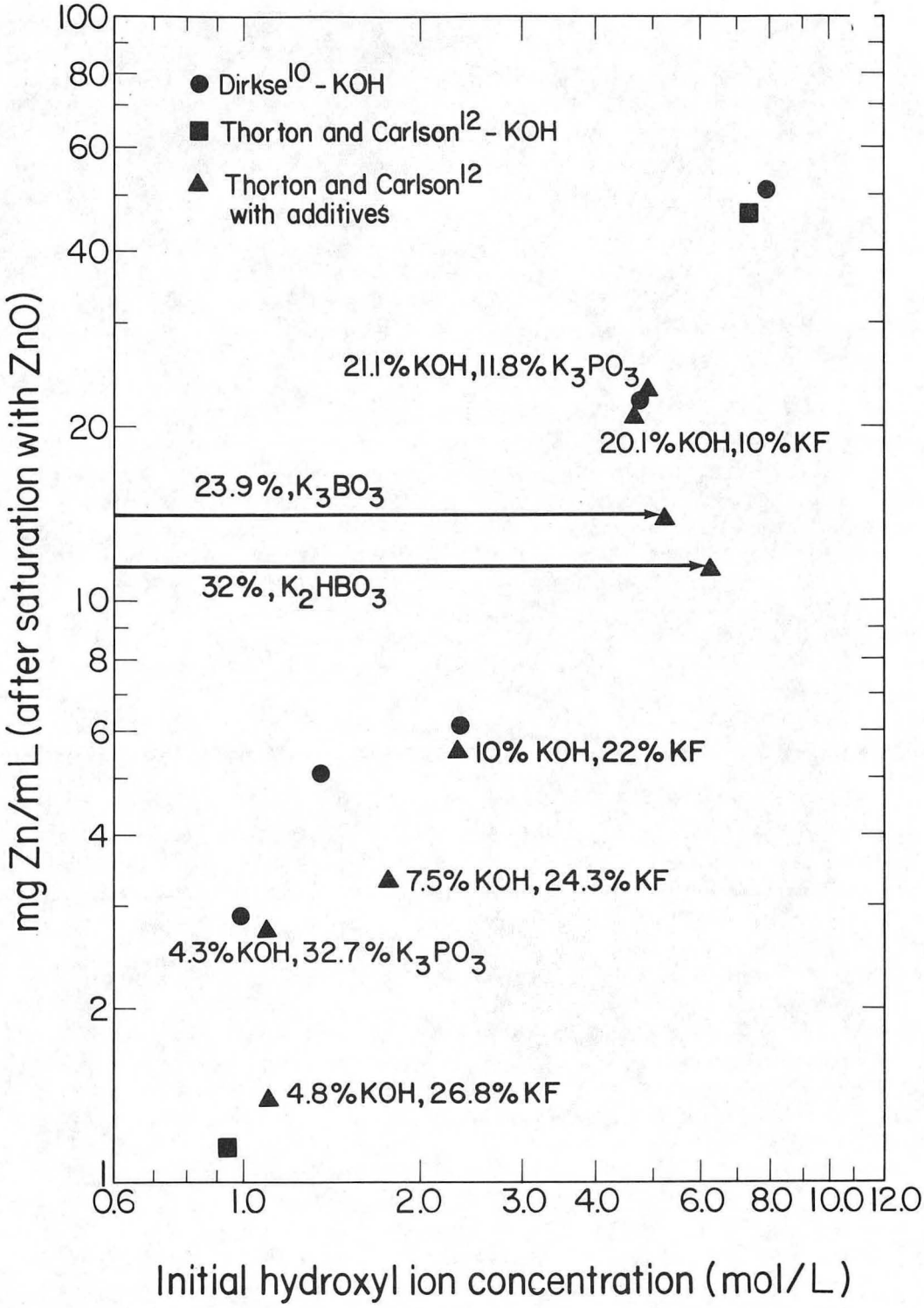

XBL 834-1666

Fig. 2

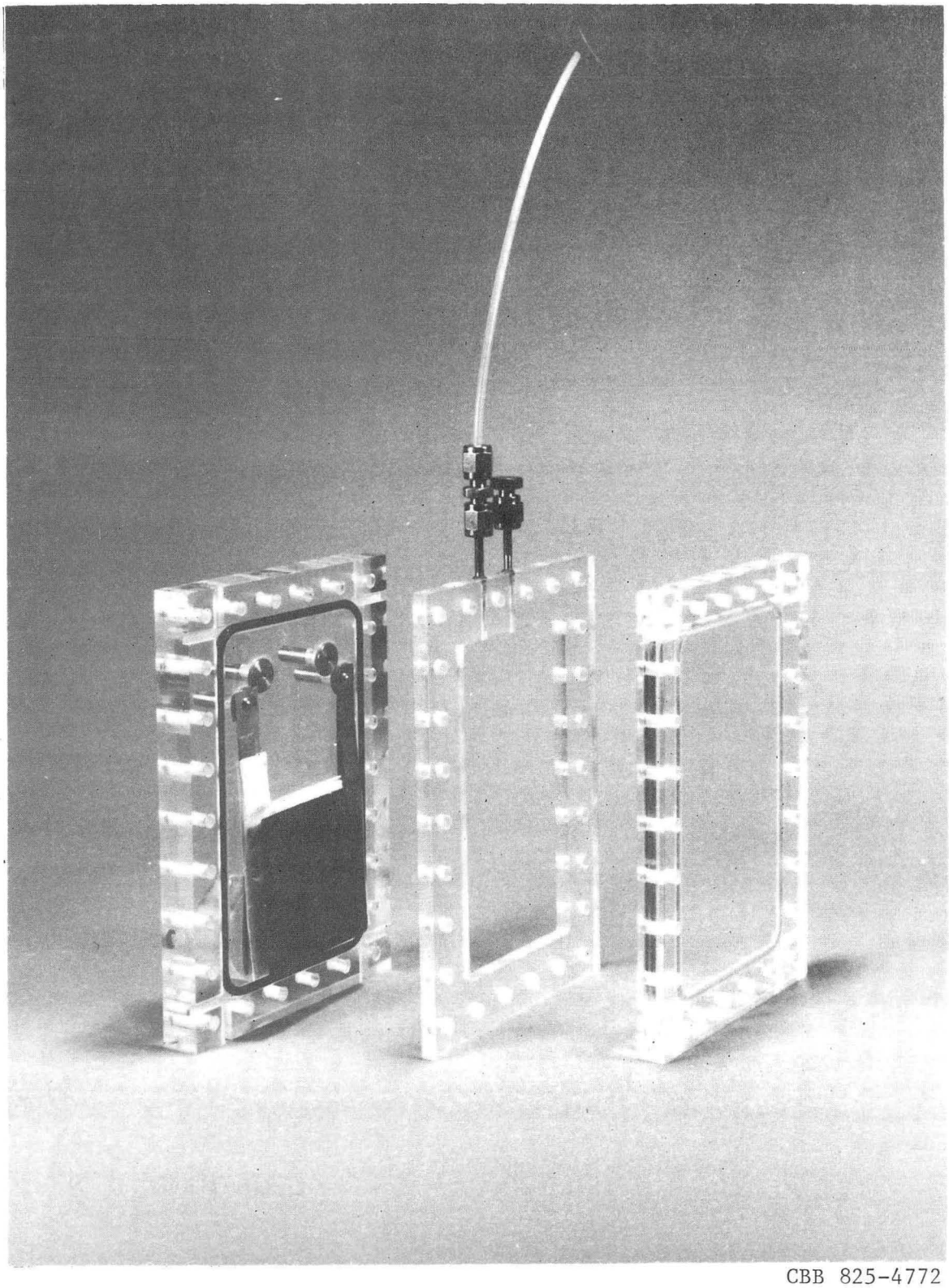

CBB 825-4772

Fig. 3

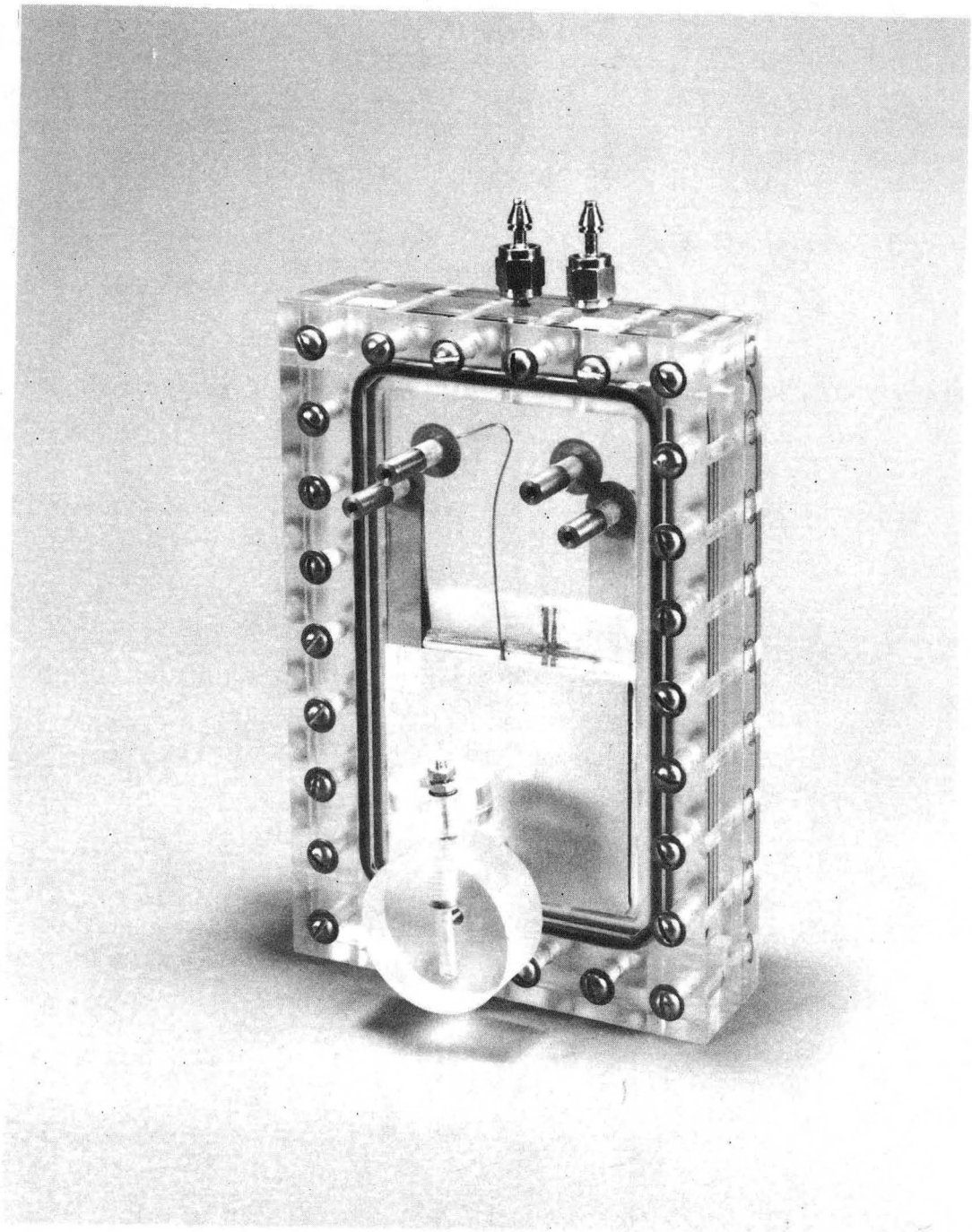

CBB 825-4774

Fig. 4

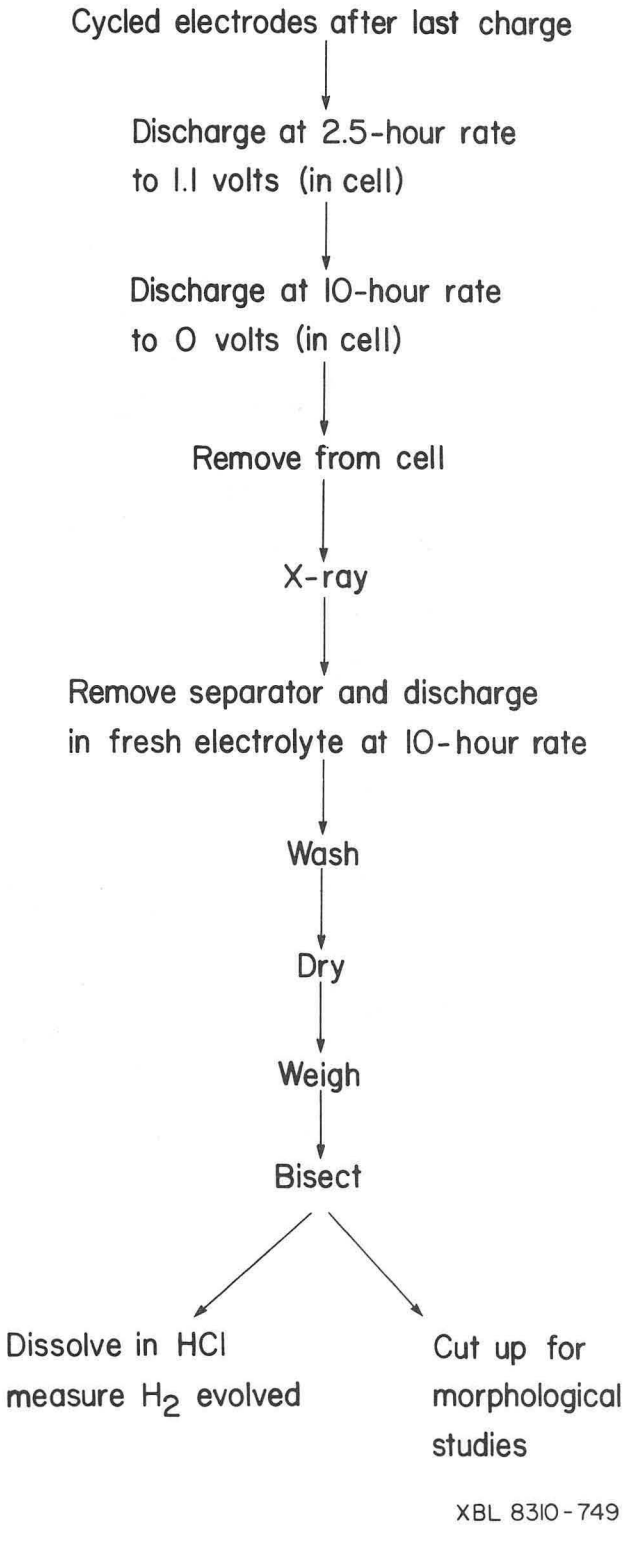
Cycled electrodes after last charge
Discharge at 2.5-hour rate to 1.1 volts (in cell)
Discharge at 10-hour rate to 0 volts (in cell)
Remove from cell
X-ray
Remove separator and discharge in fresh electrolyte at 10-hour rate
Wash
Dry
Weigh
Bisect
Dissolve in HCl measure H_2 evolved
Cut up for morphological studies
XBL 8310-749

Fig. 5

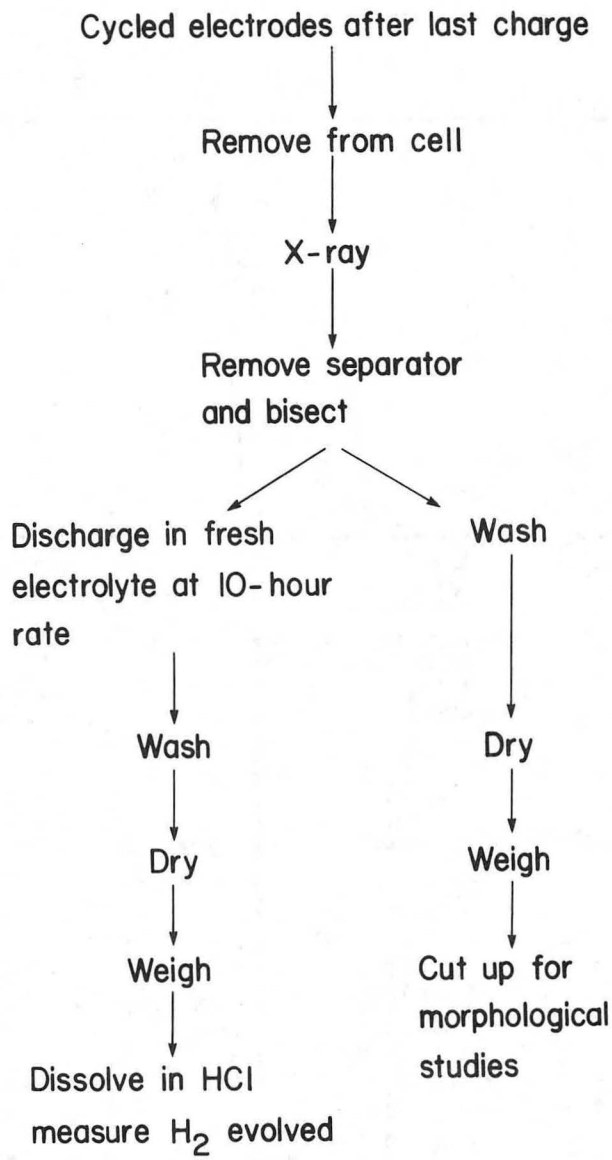

XBL 8310-3314

Fig. 6

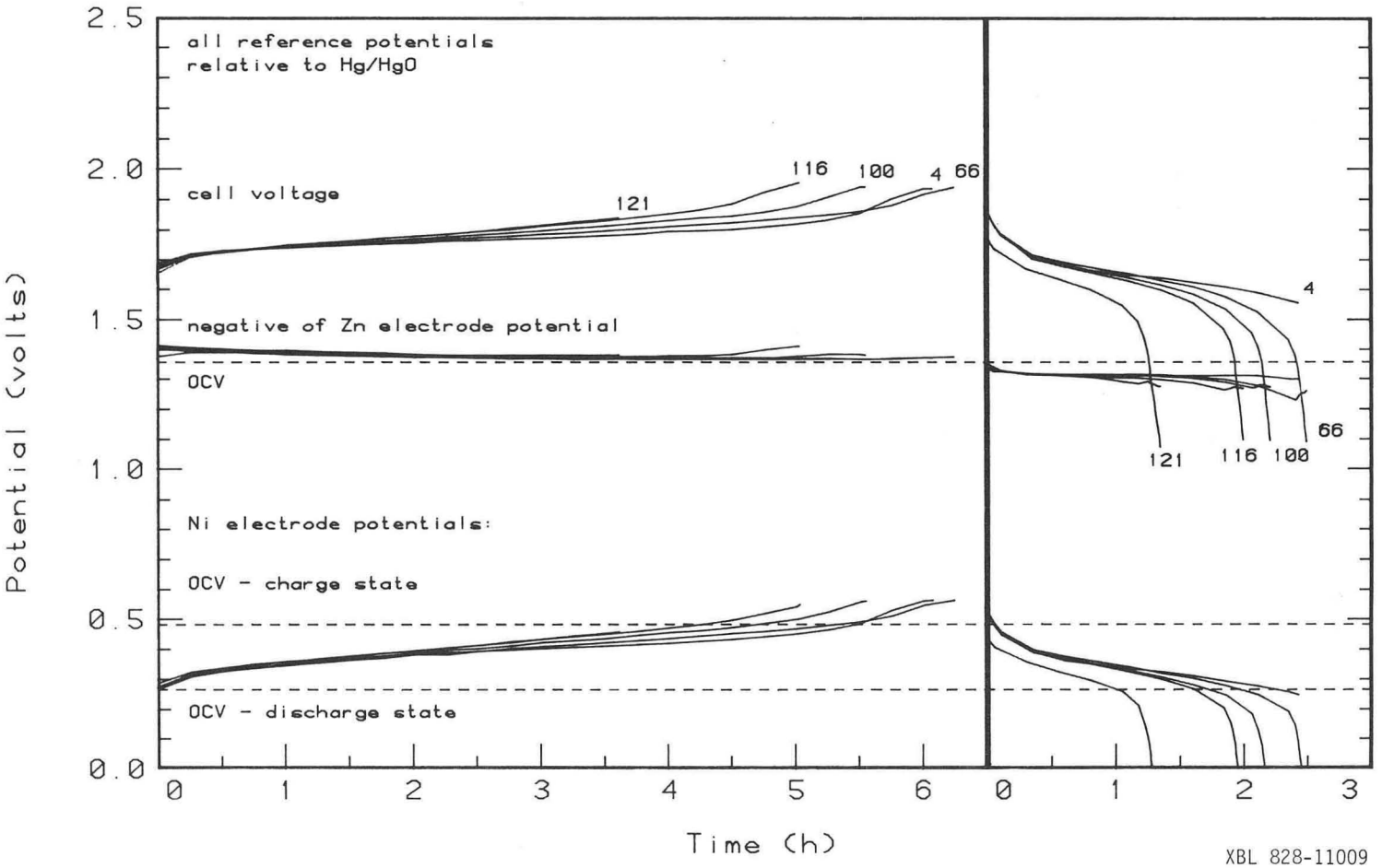

XBL 828-11009

Fig. 7

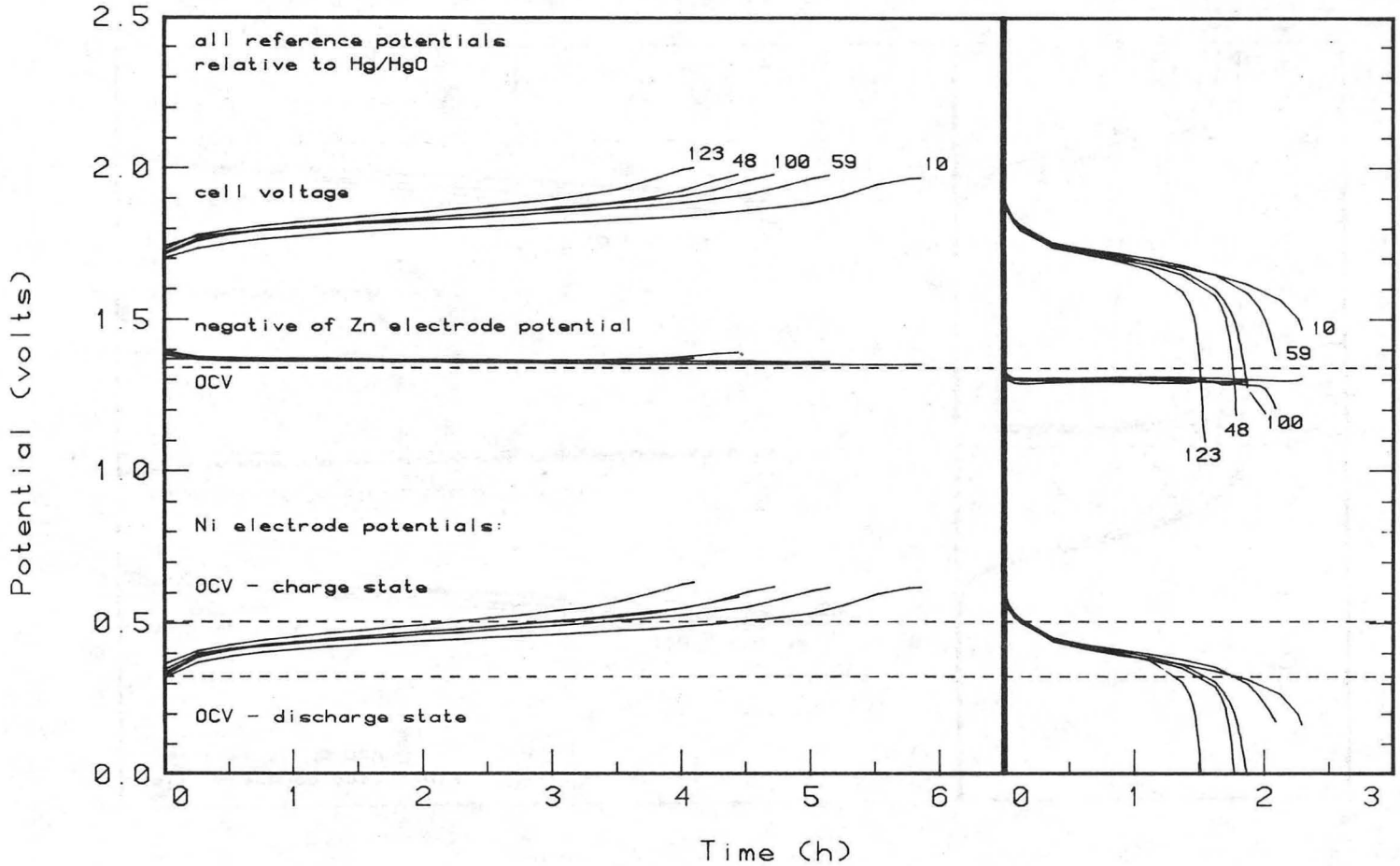

XBL 828-11010

Fig. 8

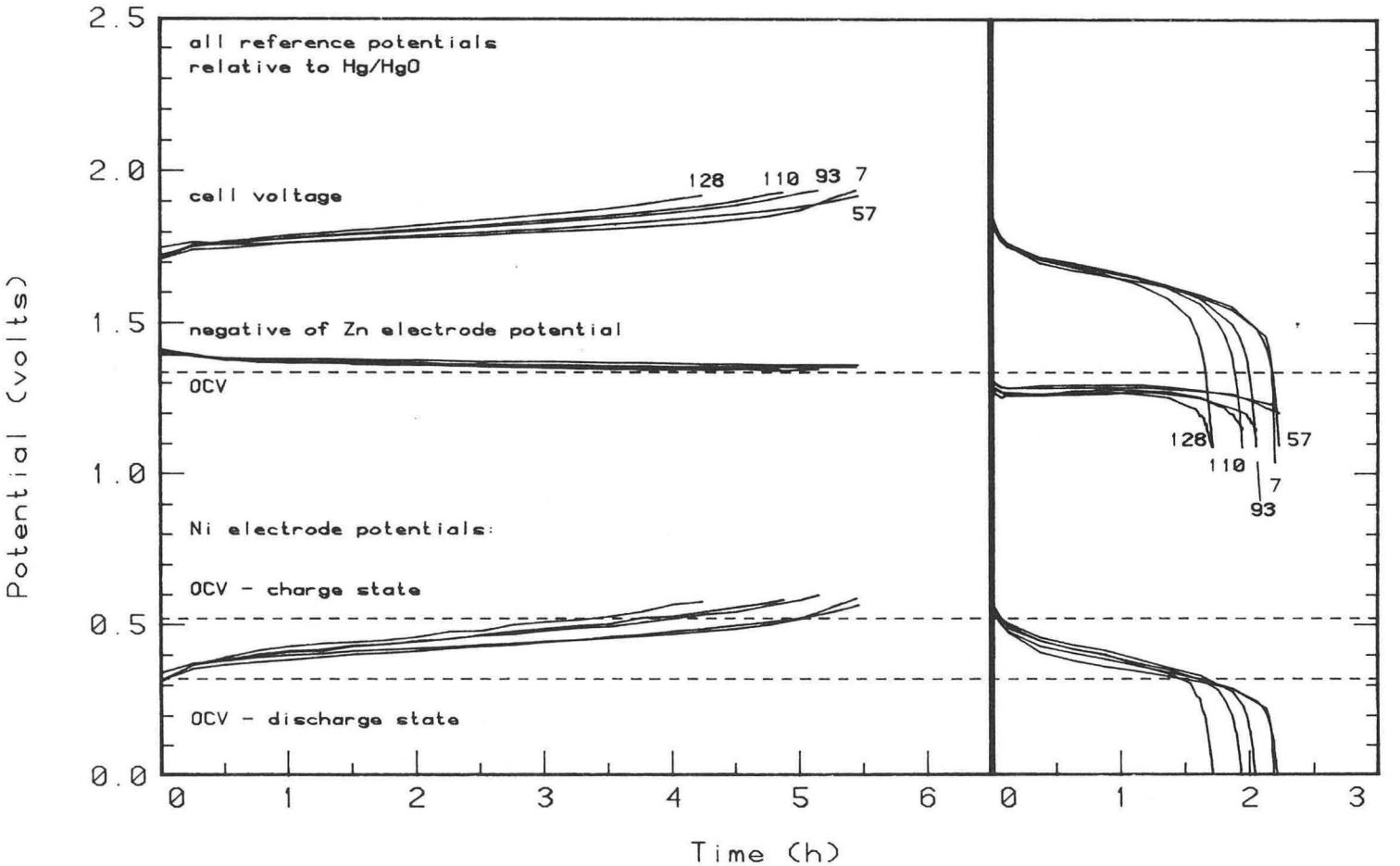

XBL 828-11004

Fig. 9a

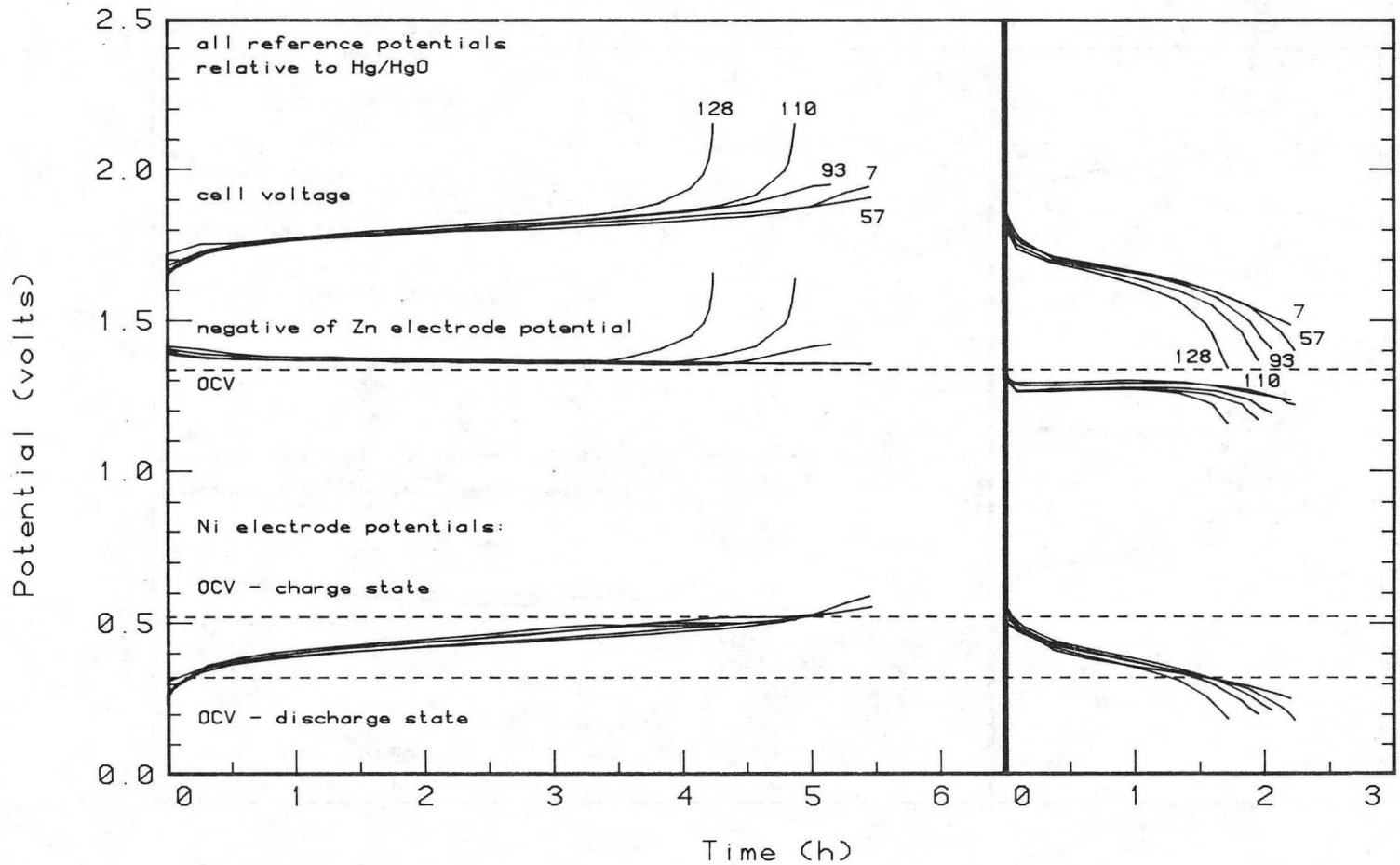

XBL 828-11006

Fig. 9b

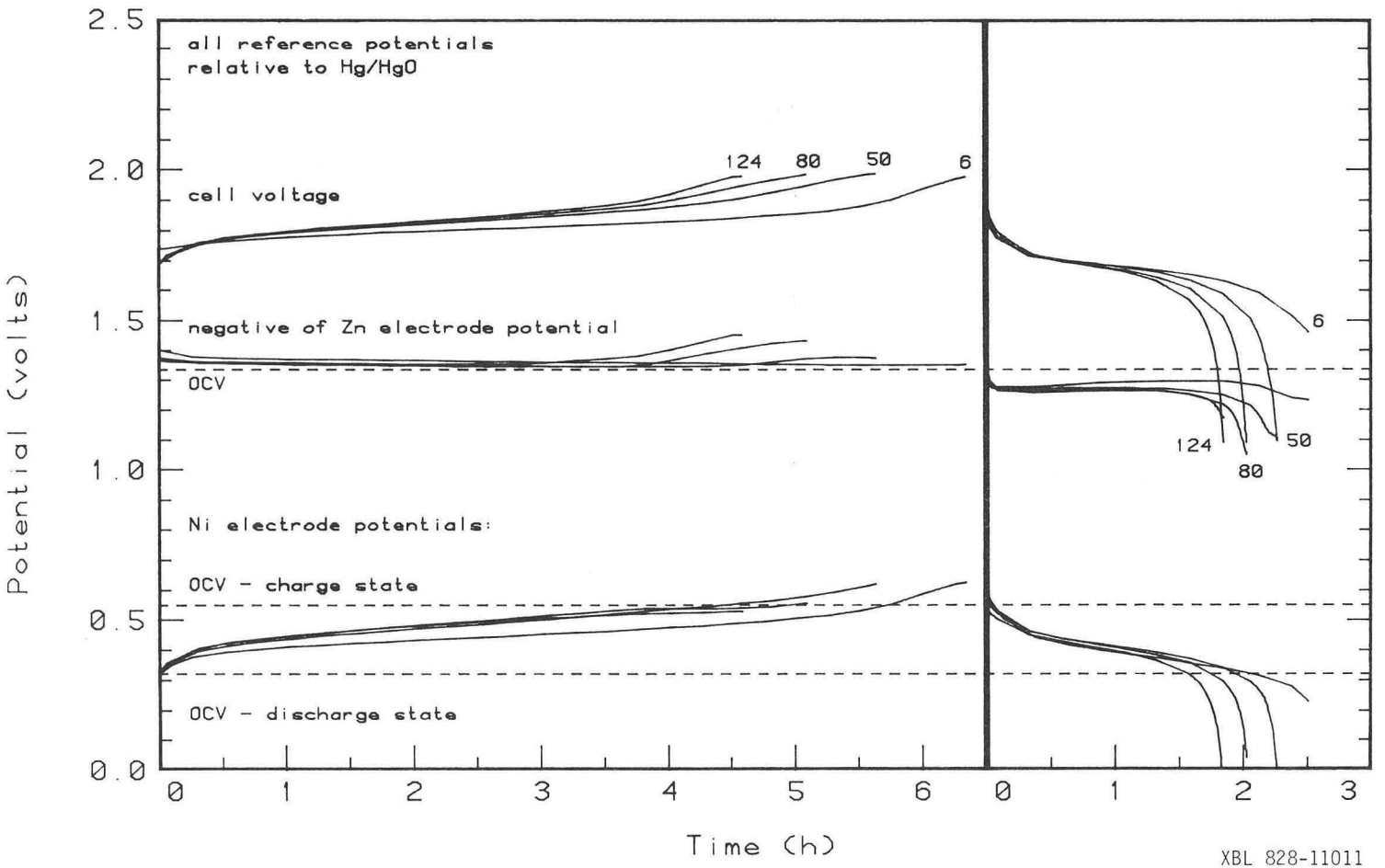

XBL 828-11011

Fig. 10

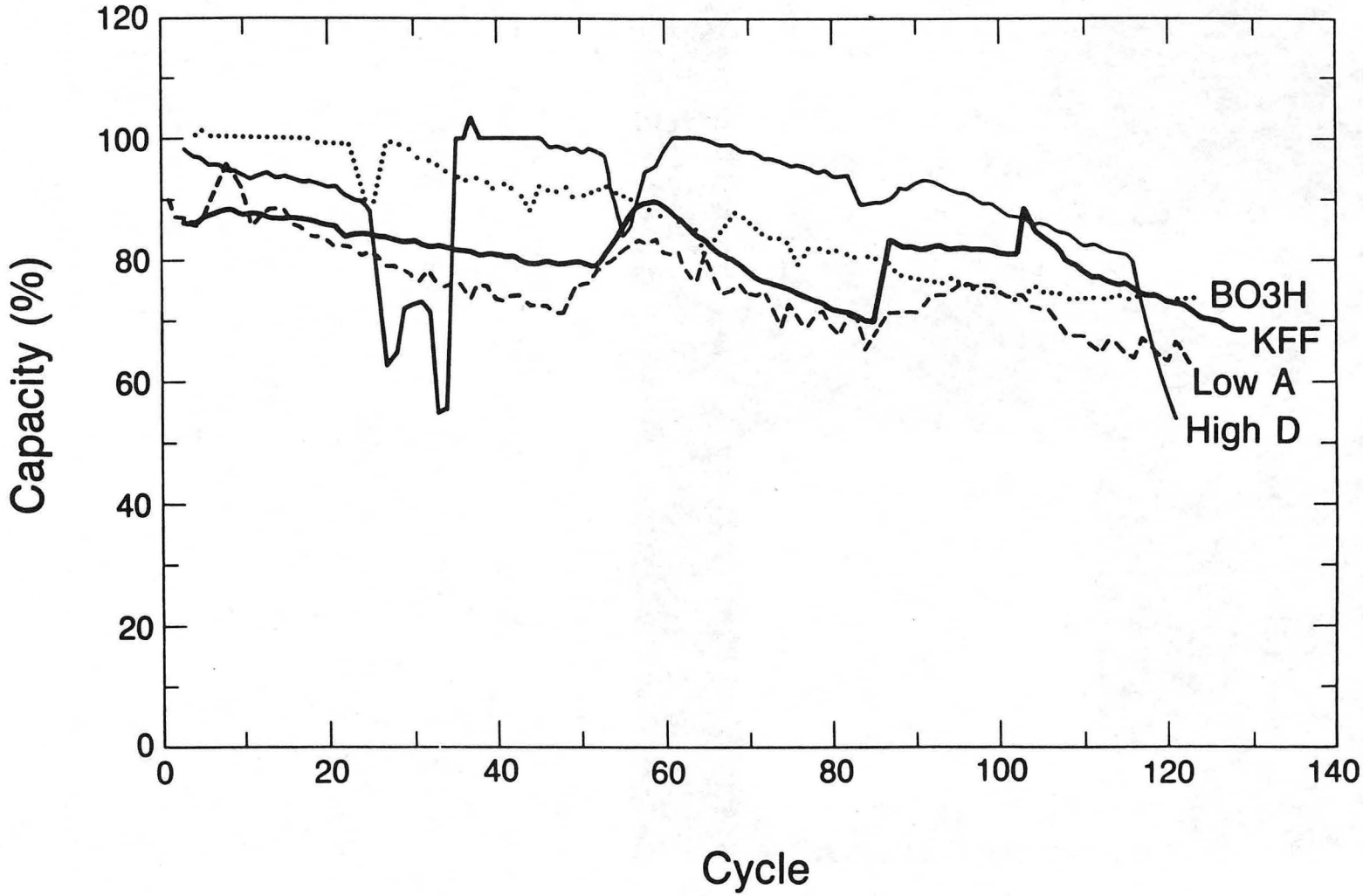

XBL 8410-4101

Fig. 11

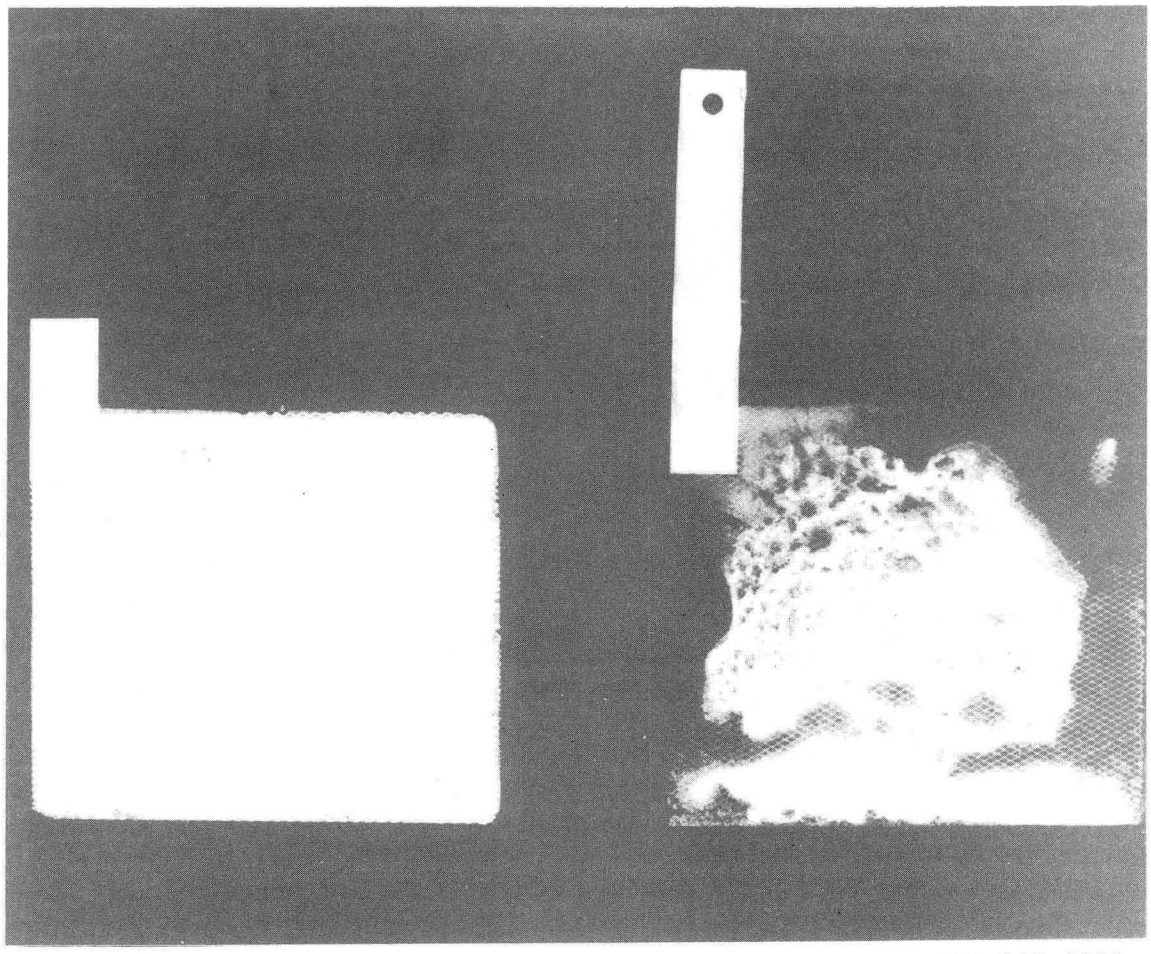

XBB 827-6073

Fig. 12

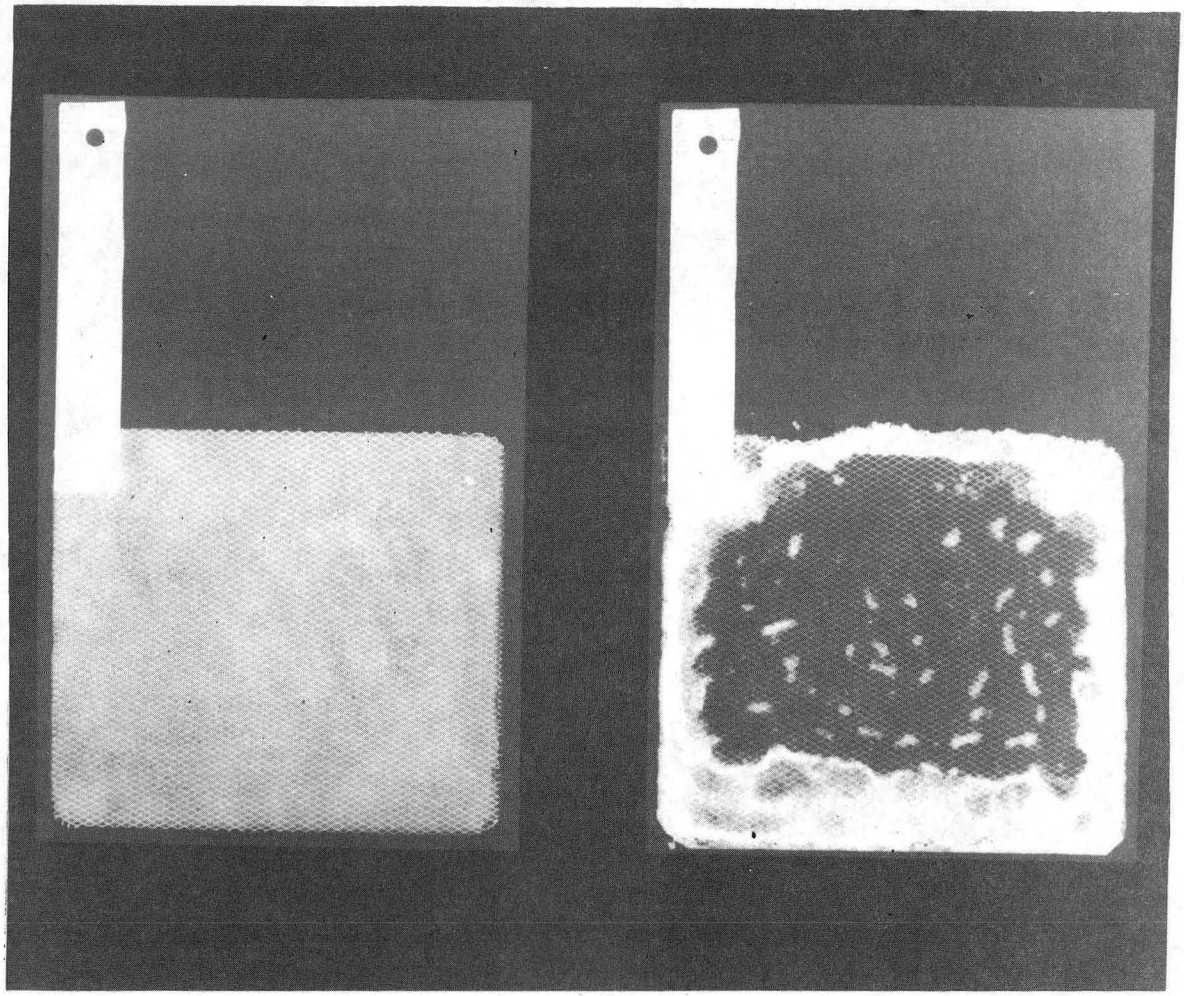

XBB 827-5924

Fig. 13

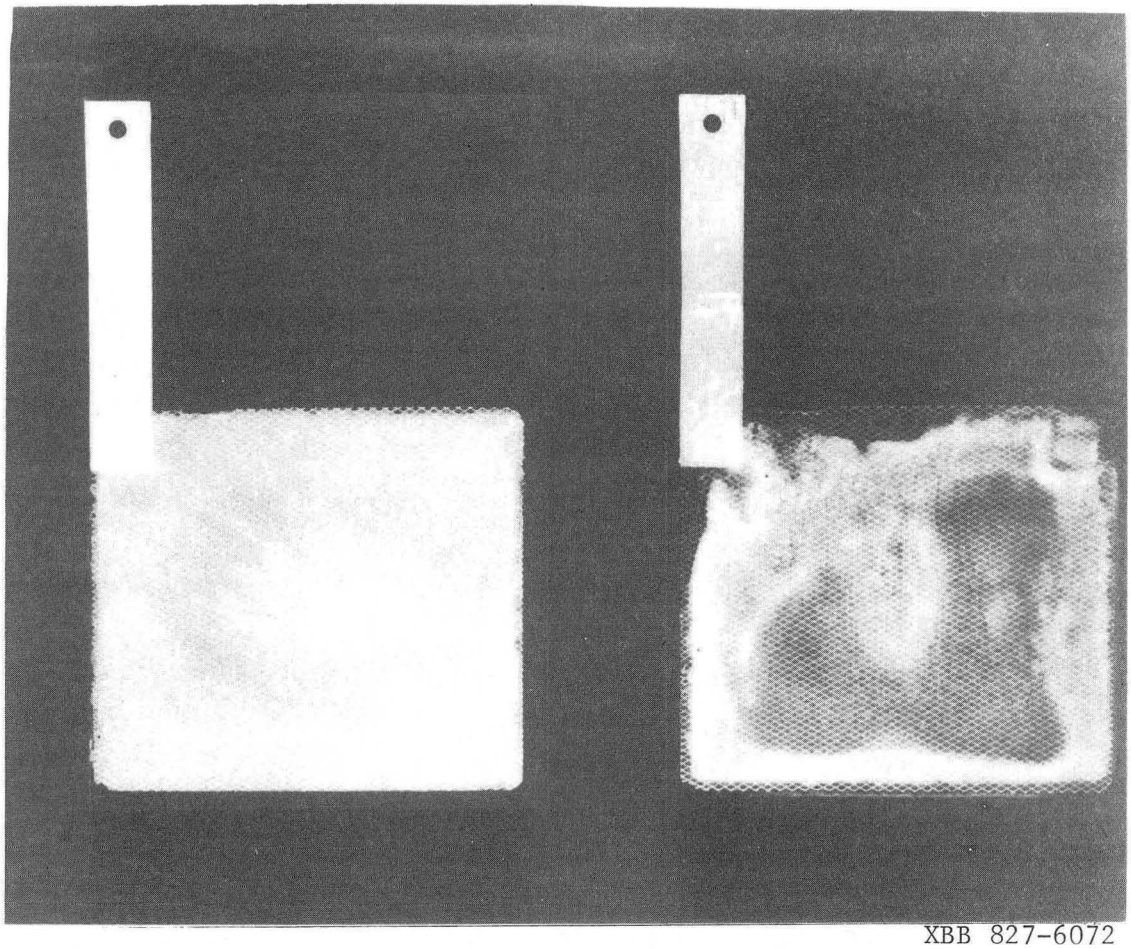

XBB 827-6072

Fig. 14

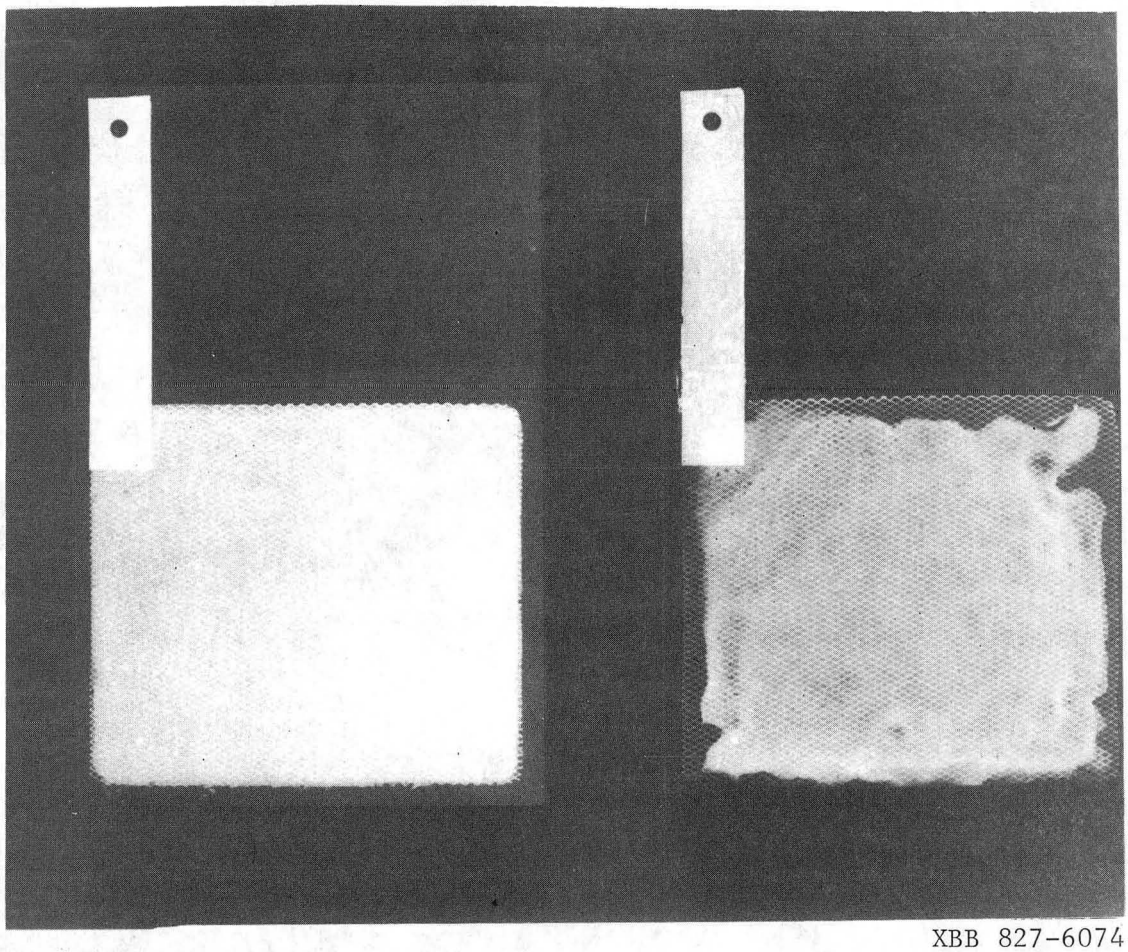

XBB 827-6074

Fig. 15

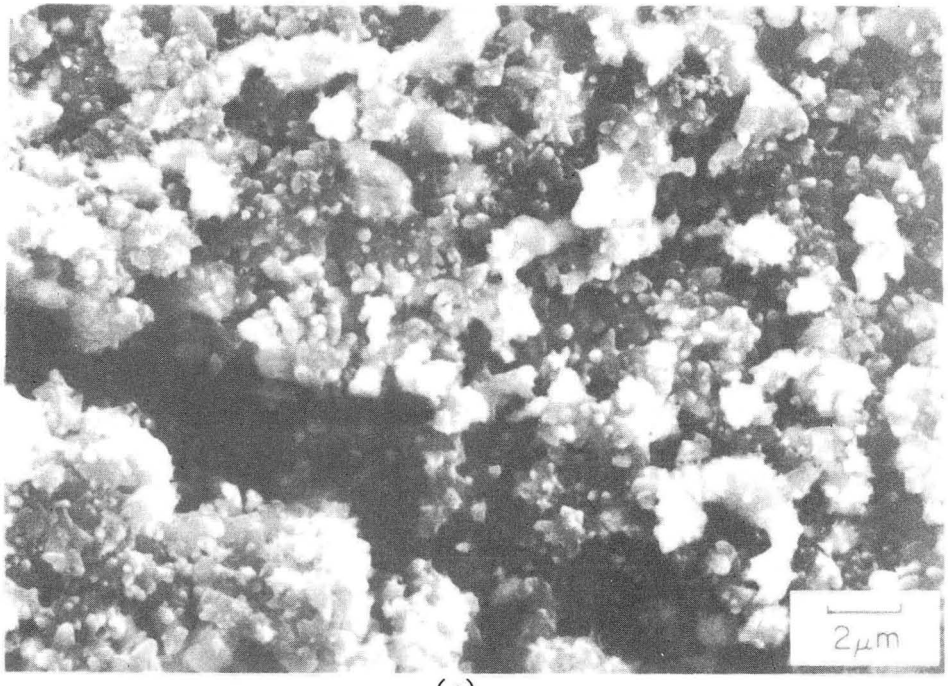

(a)

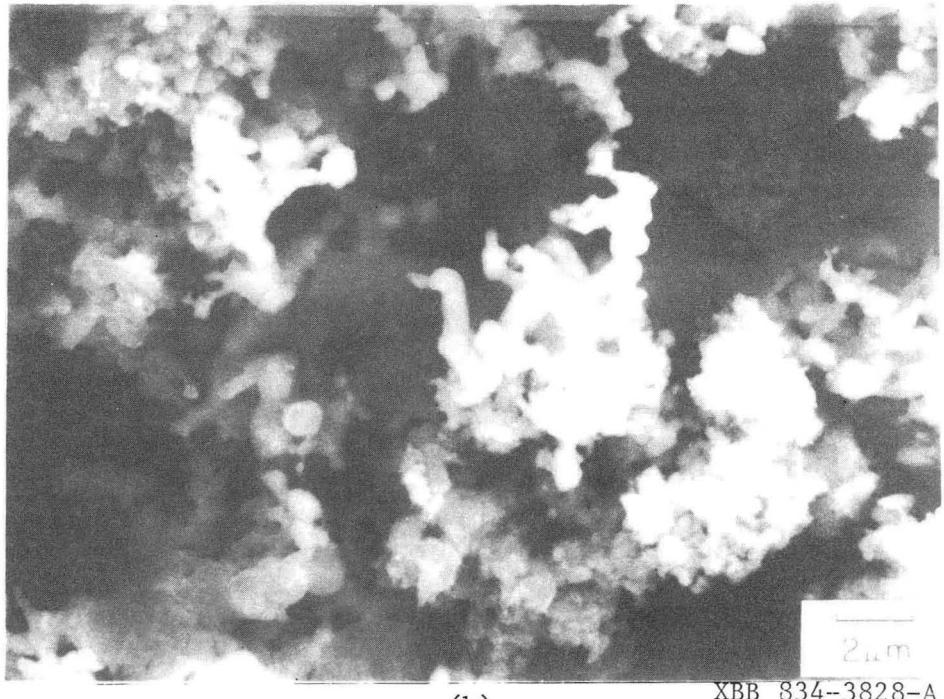

(b)

XBB 834-3828-A

Fig. 16

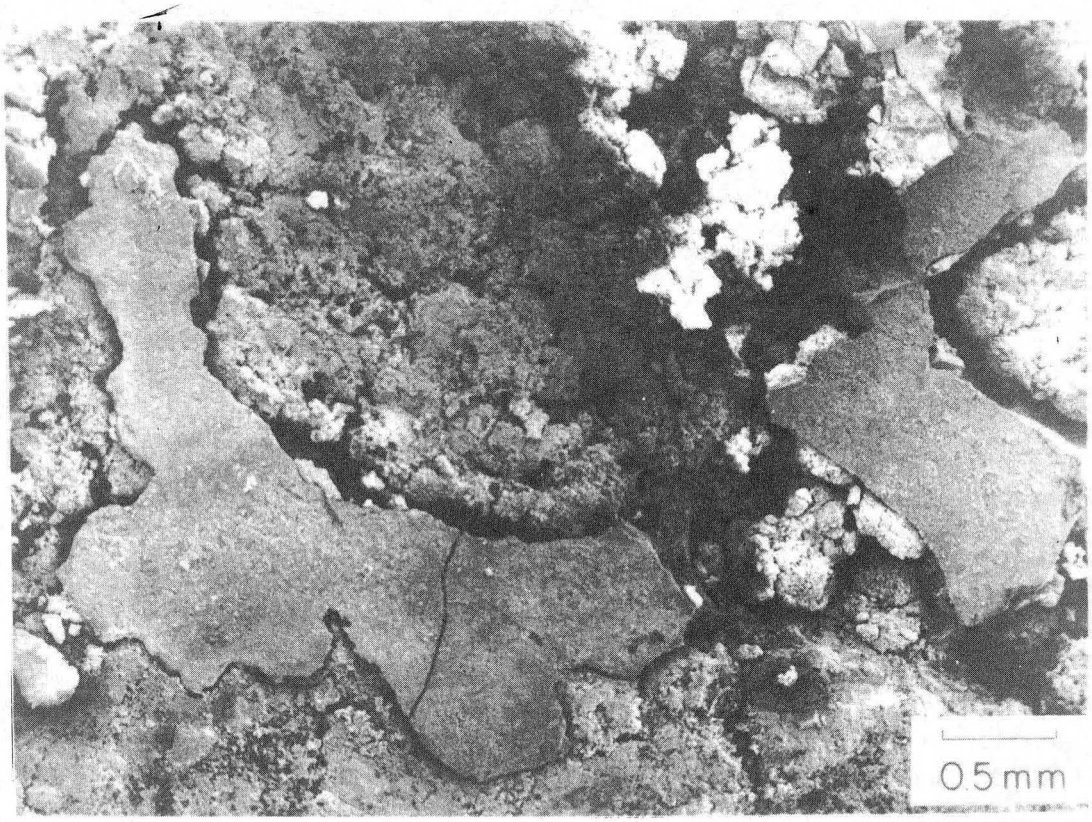

XBB 834-3829-A

Fig. 17

This report was done with support from the Department of Energy. Any conclusions or opinions expressed in this report represent solely those of the author(s) and not necessarily those of The Regents of the University of California, the Lawrence Berkeley Laboratory or the Department of Energy.

Reference to a company or product name does not imply approval or recommendation of the product by the University of California or the U.S. Department of Energy to the exclusion of others that may be suitable.

TECHNICAL INFORMATION DEPARTMENT
LAWRENCE BERKELEY LABORATORY
UNIVERSITY OF CALIFORNIA
BERKELEY, CALIFORNIA 94720